ULTRA WIDEBAND ANTENNA ARRAY PROCESSING UNDER SPATIAL ALIASING

A Dissertation

by

ALIREZA SHAPOURY

Submitted to the Office of Graduate Studies of
Texas A&M University
in partial fulfillment of the requirements for the degree of

DOCTOR OF PHILOSOPHY

August 2007

Major Subject: Electrical Engineering

ULTRA WIDEBAND ANTENNA ARRAY PROCESSING UNDER SPATIAL ALIASING

A Dissertation

by

ALIREZA SHAPOURY

Submitted to the Office of Graduate Studies of
Texas A&M University
in partial fulfillment of the requirements for the degree of

DOCTOR OF PHILOSOPHY

Approved by:

Chair of Committee,	Erchin Serpedin
Committee Members,	Deepa Kundur
	Mladen Kezunovic
	Michael T. Longnecker
Head of Department,	Costas N. Georghiades

August 2007

Major Subject: Electrical Engineering

ABSTRACT

Ultra Wideband Antenna Array Processing
Under Spatial Aliasing. (August 2007)
Alireza Shapoury, B.S., Shahid Beheshti University of Iran;
M.S., Iran University of Science and Technology
Chair of Advisory Committee: Dr. Erchin Serpedin

Given a certain transmission frequency, *Shannon spatial sampling limit* defines an upper bound for the antenna element spacing. Beyond this bound, the exceeded ambiguity avoids correct estimation of the signal parameters (i.e., *array manifold crossing*). This spacing limit is inversely proportional to the frequency of transmission. Therefore, to meet a wider spectral support, the element spacing should be decreased. However, practical implementations of closely spaced elements result in a detrimental increase in electromagnetic mutual couplings among the sensors. Furthermore, decreasing the spacing reduces the array angle resolution. In this dissertation, the problem of Direction of Arrival (DOA) estimation of broadband sources is addressed when the element spacing of a Uniform Array Antenna (ULA) is inordinate. It is illustrated that one can resolve the aliasing ambiguity by utilizing the frequency diversity of the broadband sources. An algorithm, based on Maximum Likelihood Estimator (MLE), is proposed to estimate the transmitted data signal and the DOA of each source. In the sequel, a subspace-based algorithm is developed and the problem of order estimation is discussed. The adopted signaling framework assumes a subband hopping transmission in order to resolve the problem of source associations and system identification. The proposed algorithms relax the stringent maximum element-spacing constraint of the arrays pertinent to the upper-bound of frequency transmission and suggest that, under some mild constraints, the element spacing can

be conveniently increased. An approximate expression for the estimation error has also been developed to gauge the behavior of the proposed algorithms. Through confirmatory simulation, it is shown that the performance gain of the proposed setup is potentially significant, specifically when the transmitters are closely spaced and under low *Signal to Noise Ratio* (SNR), which makes it applicable to license-free communication.

To My parents, Nayereh and Kazem, my sister Iran and my wife Nusha.

ACKNOWLEDGMENTS

I would like to express my deep gratitude to my advisor Professor Erchin Serpedin for giving direction to my research and shaping my dissertation.

I would like to thank Professor Costas N. Georghiades for his thoughtful discussions and his support during my studying and in particular during the time I was framing the problem. I am also grateful to Professor Mladen Kezunovic for the opportunity that he provided to work on an interesting and yet challenging applied research problem at Power Systems Engineering Research Center (PSERC).

I am indebted to Professor Michael T. Longnecker and his group at the Department of Statistics, who were always available to resolve the questions that I had, in the sometimes confusing world of statistics.

My special thanks are due to Professor Deepa Kundur for her proactive support during my doctorate candidacy.

I would also like to thank my good friends from Iran and around the world for their constant encouragement and emotional support during my entire doctorate study. My dear friend, Dr. Dariush Ehsani, merits particular acknowledgement for his constructive suggestions, which improved the quality of the manuscript.

Finally, I would like to express my appreciation towards my parents, Nayereh and Kazem, my sister Iran for supporting my education. I owe them all that I have ever accomplished. My heartfelt thanks go to my lovely wife, Nusha, who appreciates the quest for knowledge and has shouldered with me the joyous burden of seeing my doctoral studies through.

TABLE OF CONTENTS

CHAPTER Page

LIST OF TABLES

LIST OF FIGURES

FIGURE Page

CHAPTER I

INTRODUCTION

A. Motivation

The recent promises for relaxing the regulations regarding the wideband application of the commercial wireless systems revived the classic studies and sparked a new wave of wideband processing. The new FCC regulations seem to favor a wider transmission bandwidth by expanding license-free spectrums, thanks to the recent advances in manufacturing technology of low power communication systems [1].

Prompted by this development, many industries and institutes started investigating the use of license-free transmissions. For instance, Power Systems Engineering Research Center (PSERC) initiated a project to explore the possibility of replacing the prohibitively expensive instrumentation and control wirings in the electric power substations, with the wireless solutions [2]. Several comprehensive field measurements and statistical analysis have been performed for this purpose [3, 4, 5], which *inter alia*, suggests that the wireless channels in ISM spectrum tend to be more *interference–limited* than *noise–limited* in particular in residential regions, where the wireless devices are growing in abundance.

We can of course assume man-made interferences are *independent and identically distributed* (i.i.d.) and hence consider them as an additive Gaussian constituent according to the *Central Limit Theorem* (CLT). Nonetheless the empirical measurements indicate that this assumption may not hold true *globally over time* as the interferences exhibit a time-dependant pattern and require a more elaborate model, based on time series analysis (See Appendix A).

The journal model is *IEEE Transactions on Automatic Control.*

This finding further signifies that the wireless instruments are more competing against each other for the spectrum over the time, rather than against the noise.

In this regard, beamforming and array steering seem to be the panacea of the high data rate wireless networks. For instance in [6], it is shown that that even with full knowledge of network and perfect scheduling of the nodes, the throughput of the multi-hop wireless network decreases as the number of nodes in the network increases, making the wireless network *unscalable*.

It is further suggested that utilizing the *spatial diversity* in the antennas, e.g., *beamforming* or utilizing *phased arrays antennas*, will be advantageous in increasing the spatial concurrency of transmission and hence increasing the capacity, since the wireless network links would then act as wired ones enabling the scalability, while offering more transmission security due to the arrays' directive nature[1].

Wideband array processing was extensively discussed in several publications during the past three decades, striving for better performance and error-free communication (see [8] for additional references). On the implementation side, the errors of the array antenna are seldom due to mechanical tolerances or inaccurate element spacings [9]. The main imperfections are due to less discernible factors such as mutual coupling which impact both phase and the amplitude of the excitation, and uncertain and sometimes nonlinear impulse response of the communication network, particularly in broadband scenarios.

It is generally known that the element spacing of the arrays, d, should be $d < \lambda_{min}/2$ or $d < c/2f_{Max}$ to avoid *spatial ambiguity* in an all-angle array processor (λ_{min} and f_{Max} stand for the minimum wavelength and the maximum frequency

[1]Some researchers (e.g., Grossglauser and Tse [7]) calculated the network capacity considering other sets of assumptions, however under practical scenarios, the network capacity is still bounded, unless more diversities are utilized.

of the wideband system respectively, and c is the propagation velocity). Hence, a wideband system with high frequency mandates tightly packed arrays or smaller spacings, which increase the mutual coupling between the elements and adversely decrease the communication capacity [10, 11, 12, 13].

In array literature, arrays that are designed with the maximum *all-angle* spacing $d = \lambda/2$ are called *standard arrays*. If we limit our angular range, we can design arrays with $d/\lambda > 0.5$ (i.e., higher frequencies than the standard frequency of the array). For instance, if we limit the scanning range to $(-30°, 30°)$, we can still avoid aliasing with an array with $d/\lambda \cong 1$ since the *grating lobes* occur outside of the scanning range.

In most broadband (or wideband) processing in ULA's, the arrays are considered such that the center frequency of the transmission band coincides with the standard frequency of the array [14, 15, 16]. This still would permit non-aliased analysis of the system, even if the fractional bandwidth is more than 40 percent of the center frequency but under the constraint of limiting the scanning angle.

A different approach was presented in [17], where the array processor could resolve the ambiguity problem within a defined sector of interest in the scanning angle. To remedy the limitation on the scanning angle range, one may design the array so that the standard frequency of the array coincides with the lower limit of the spectral support. In this case, although there is no aliasing, there are two drawbacks: the necessity of decreasing the element spacing, which produces undesirable electromagnetic couplings (and consequently a reduction of network capacity), and limitation of array resolution [18, 19]. Herein, we assume plane waves *resolvable*, if the peak of the second beam pattern lies at or outside of the null of the first beam pattern (i.e., separation is greater than or equal to BW_{NN}, where BW_{NN} is null-to-null bandwidth of the beam pattern). The exact definition comes from the *Rayleigh Resolution Limit*

which is defined as

$$\theta = 2\sin^{-1}(\frac{1}{M(\frac{d}{\lambda})}) \ , \tag{1.1}$$

where M is the number of elements in the array.

One possible way of avoiding the spatial aliasing, while maintaining a good resolution and accepting an increased (however average) element spacings, is to design sparse linear arrays with uniform or nonuniform element spacing. These arrays often exhibit high side–lobes and are difficult to adopt for broadband applications. There are many references that address the estimator ambiguity and the identifiability issues of these arrays (see e.g., [20, 8, 19] and their references). Many of these arrays are extensions of the commonly considered ULA, which is discussed in this dissertation.

B. Background

In array signal processing, we are mainly exploiting the coherency of the signal in space in order to discriminate against noise. Figure 1 shows a typical disposition of a linear array with 14 elements. We assume that the wave propagation is planar, which enables us to model the transmitters and the elements of the array in the same plane. Furthermore we assume that the channel is homogeneous and is not dispersive and there is a linear medium throughout the array length. We also consider that the elements have almost the same angle to the transmitter. Under these assumptions, the wavefront of the transmitted signal from the source would be coherent and what is received at the various sensors is identical in form, except for a *valuable* time delay. If the wave travelling speed is c and the spacing between the elements is d then the m^{th} element receives the wave with τ_m delay with respect to the first element in the

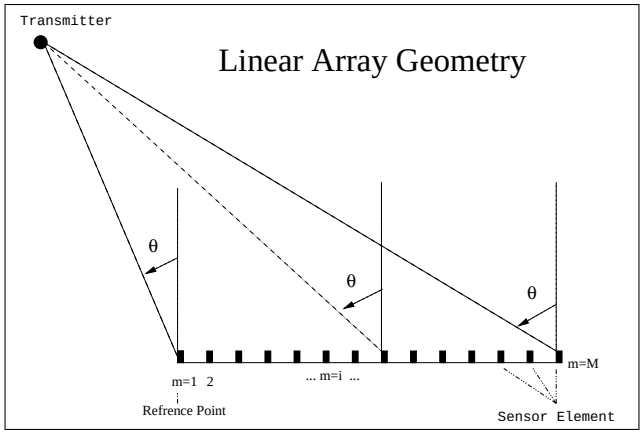

Fig. 1. Disposition of a uniform linear array.

array (i.e., reference point). Hence[2]

$$\tau_m = (m-1)\frac{d\sin(\Theta)}{c} \ , \tag{1.2}$$

where $\Theta \in (-90, 90)$ is the angle of the transmitter(s). The relative phase difference between two adjacent sensor elements, that for instance receive a single-tone signal having the wavelength λ (and angular frequency of ω rad/sec) arriving from angle θ, is given by:

$$\phi = \omega\tau_1 = \omega(\tau_2 - \tau_1) = \ldots = 2\pi\frac{d}{\lambda}\sin(\theta) \ . \tag{1.3}$$

In ULA with a visible range of $(-90°, 90°)$, if the element spacing d is greater than the half-wavelength $(\lambda/2)$, the grating lobes may occur within the visible scanning range, which produces the spatial aliasing, i.e., a phenomenon similar to the Nyquist or Shannon temporal aliasing caused by undersampling of the waveforms in time series analysis.

[2]As explained in Appendix B, the same delay calculations can be easily extended to the 3-D scenario using the rectangular or spherical coordinate system and elementary geometry.

1. Broadband Design for Phased Array Systems

There are in general two main issues in designing a phased array system for broadband data communication which are closely related to each other. The first one is the wideband antenna design. Although the wideband antennas have already been used for radar applications for decades, the literature is scanty for data communication purposes.

Broadband octave nested arrays are studied in [21, 22]. Nested arrays are compound arrays consisting of a nested set of sub-arrays. Each of these sub-arrays is then designed for single frequency (one octave). Figure 2 shows a nested array with three 9-element subarrays ($M = 9$) at each octave. In this case the minimum element spacing corresponds to the highest frequency, which still mandates a packed array structure. Furthermore the required number of elements in this setup is prohibitively high. For instance, the broadband nested array in Figure 2 requires $M + 3(M + 1)/2 = 26$ total elements. The other disadvantage of this broadband arrays is the limited (and fixed) set of frequency band ratios (octave ratio). In other publications [23, 24] wideband antennas, applicable to wireless networking were discussed in which multi-octave band planar slot line arrays have been designed for high frequency wireless networking. The drawback of these antennas are the limited scanning angle of ± 30 degrees.

The second issue in broadband design is the wideband array signal processing. On the processing side, the literature has gone through several phases of evolution, in particular has evolved from narrowband processing. Many researchers have tried to use the already–developed narrowband algorithms and fuse the data of several narrowband estimations to perform wideband implementations.

There are two methodologies to implement the fusing task, coherent and incoherent combining. The incoherency here means that no combining is performed until the

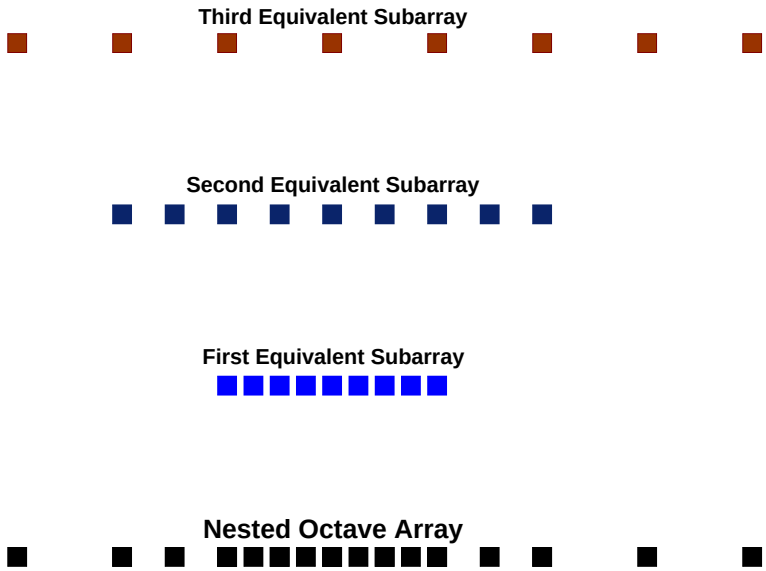

Fig. 2. A typical broadband octave nested array.

data from each band is processed by a nonlinear processor. In the coherent approach on the other hand, the data coming from all bands are processed at once. In [25] the incoherent approach is addressed, while in [15], it is argued that the errors increase dramatically at low SNR in the case of incoherent combining and suggested an alternative coherent approach to overcome this limitation. The tendency to reject the incoherent approach is mainly due to the inaccuracy of the order estimation problem (i.e., number of sources) in these methods.

Aside from the combining methodologies, adaptive array processing can be categorized into general groups such as spatial only (e.g., [14]), gradient based algorithms [26], subspace methods such as MUSIC [18], ESPRIT [27], BASS-ALE [28] estimation etc.. Each method presents its own drawbacks and advantages compared to the others and the practical performance of the methods in a certain application sets the

superiority.

The main contribution of this work is the combined estimation of the transmit data signals and the *Direction Of Arrival (DOA)* beyond the *Shannon Spatial Sampling Limit* using ensemble frequency diversity, which is achieved by a *subband hopping* scheme.

Although we are not aware of similar studies addressing our problem, we base our approach mainly on the previously developed researches in this area and render it amenable to our topic.

Herein it is assumed that the transmitter power is fixed for all subbands and the elements have almost the same angle to the transmitter, i.e., the *far-field assumption* holds. It is found that given an appropriate wideband communication scheme, one can resolve the spatial ambiguities in the direction of arrival estimation even if the antenna element spacing is larger than the above mentioned limit.

C. Outline

The organization of this work is as follows. Chapter II formulates the problem and develops its mathematical model. This model is used in Chapters III and IV to develop a wideband approach. This section constitutes the main body of our work as it discusses the constraints and the methodology for resolving the spatial aliasing. In Chapter III, we propose an MLE-based algorithm. In Chapter IV, a suboptimal approach similar to the well-known MUltiple SIgnal Characterization (MUSIC) [18] is proposed and is shown to be amendable to the wideband scenario. The error magnitudes of the algorithms are discussed in Chapter V and an approximate formula for the error is proposed. Then results are compared to the error approximate formula through confirmatory computer simulations in Chapter VI.

CHAPTER II

PROBLEM SETUP

A. The Mathematical Model

The wideband signal model considered in this work is considered to be a sum of disjoint narrow frequency bands. This is actually a popular method for wideband array processing [29, 15, 25, 14, 30]. A ULA is assumed with M omnidirectional antenna elements with element spacing d. The broadband communication is implemented using a finite number of *narrowband* plane-waves impinging on the array. Each narrowband plane-wave, which is referred to as a *subband* in this correspondence, is assumed to have a spectral support of B Hz. All transmitter sources use fast-subband hopping with the hopping duration of T_h. During each hop, the source k, which is at azimuthal direction θ_k relative to the broadside of the array, transmits using L subbands with center frequencies $\{\omega_{k1}, \omega_{k2}, \ldots, \omega_{kL}\}$, respectively, and $\delta = \min(\omega_{ki} - \omega_{k(i-1)}) = 1/T_h$ to obtain efficient utilization of the frequency spectrum. Let us suppose that we have just one source and drop any k subscript for notational convenience. In Section D, the problem of having $k \in [1, K]$ subband hopping sources impinging on the array is investigated, where a set of disjoint subbands is used for transmit sources. The signal received by the m^{th} element of the array, from the subband hop l, can be expressed as:

$$u_{m,l}(t) \;=\; Q_{ml}(\theta) s_l(t) + e_{m,l}(t) \;, \tag{2.1}$$

or in matrix format:

$$\mathbf{U} \;=\; \mathbf{Q}(\theta)\; \mathbf{S} + \mathbf{E} \;, \tag{2.2}$$

where

1. The set of the frequency subbands Ω, $\{\omega_l \in \Omega \mid l \in [1, L]\}$, is assumed known by the hopping-based transmitter and receiver (L is the total number of frequency subbands).

2. $m \in [1, M]$ is the m^{th} sensor element and the total number of sensors, M, is a known constant.

3. $Q_{ml}(\theta) = \left[e^{(m-1)\omega_l[-j\frac{d}{c}\sin\theta]}\right],\ m \in [1, M], l \in [1, L]$ is the steering matrix. The column vector, i.e., $L \times 1$ matrix $Q_l(\theta)$, of the steering matrix is often referred to as the steering vector of the array or the array *manifold*.

4. θ is the parameter indicating the direction of the source and is unknown.

5. $\mathbf{S} = \text{diag}\ [s_1(t)\ , s_2(t)\ , \ldots\ , s_L(t)]$, in which $s_l(t)$ is the signal vector at each subband with spectral support of B Hz.

6. $\mathbf{E} = [e_{m,l}(t)],\ m \in [1, M], l \in [1, L]$ is the noise matrix. The noise is assumed stationary, with zero mean, Gaussian process.

B. Discussions on the Assumptions

1. Narrow-Band Assumption

Let us assume $s_l(t)$ is the baseband signal (which could be complex) and let $x_l(t)$ be the bandpass transmitted signal resulting from the *complex modulation* with carrier frequency of ω_l, i.e., $s_l(t)e^{j\omega_l t}$. The index $l \in \{1, \ldots, L\}$ refers to one of the several frequency bins which the transmitter uses to modulate the data. We later discuss the constraint on the spectrum support of signals $s_l(t)$ and on the total number of frequency bins.

Since $x_l(t)$ is a physical signal, its spectrum should be even, hence:

$$X_l(\omega) = S_l(\omega - \omega_l) + S_l^*(-\omega - \omega_l) \ , \tag{2.3}$$

where '*' denotes the complex conjugate and $X_l(\omega)$ is the Fourier transform of $x_l(t)$. $x_l(t)$ in the time domain takes the expression:

$$x(t) = 2Re\ [s(t)e^{j\omega_c t}] \ . \tag{2.4}$$

The signal impinging to the m^{th} sensor element of the array as the result of this transmission at frequency ω_l is:

$$y_{m,l}(t) = h_{m,l}(t) \mathbf{*} x_l(t - \tau_m) + e_{m,l}(t) \ , \tag{2.5}$$

or

$$y_{m,l}(t) = 2h_{m,l}(t) \mathbf{*} Re\ [s_l(t - \tau_m)e^{j\omega_l(t-\tau_m)}] + e_{m,l}(t) \ , \tag{2.6}$$

in which $h_{m,l}(t)$ is the impulse response of the channel, $e_{m,l}(t)$ is the total noise with regard to the m^{th} sensor element, τ_m is wave propagation delay between the reference element and the m^{th} element in the array, and '**' denotes the convolution. (Note that all of the above signals are physical signals.)

In the frequency domain:

$$Y_{m,l}(\omega) = H_{m,l}(\omega)X_l(\omega)e^{-j\omega\tau_m} + E_{m,l}(\omega) \ . \tag{2.7}$$

Substituting the value of $X_l(\omega)$ in equation (2.7) yields:

$$Y_{m,l}(\omega) = H_{m,l}(\omega)[S_l(\omega - \omega_l) + S_l^*(-\omega - \omega_l)]e^{-j\omega\tau_m} + E_{m,l}(\omega) \ . \tag{2.8}$$

In the demodulation part, on each of the sensor element of the array, *complex demodulation* is performed by multiplexing the received signal $y_m(t)$ with the locally

generated complex waveform $e^{-j\omega_l t}$ or:

$$v_{m,l}(t) = y_{m,l}(t)e^{-j\omega_l t} = h_{m,l}(t)\textbf{*}x_l(t-\tau_m)e^{-j\omega_l t} + e_{m,l}(t)e^{-j\omega_l t} \ . \tag{2.9}$$

The spectrum of $v_{m,l}(t)$ is:

$$V_{m,l}(\omega) = H_{m,l}(\omega+\omega_l)X_l(\omega+\omega_l)e^{-j(\omega+\omega_l)\tau_m} + E_{m,l}(\omega+\omega_l) \ , \tag{2.10}$$

$$V_{m,l}(\omega) = H_m(\omega+\omega_l)[S_l(\omega) + S_l^*(-\omega-2\omega_l)]e^{-j(\omega+\omega_l)\tau_m} + E_{m,l}(\omega+\omega_l) \ . \tag{2.11}$$

If we pass $v_{m,l}(t)$ through a low-pass filter with the bandwidth limited to the bandwidth of the signal $s_l(t)$, B_l, and assume that B_l is smaller than ω_l, then we can eliminate the component in $V_{m,l}$, which is centered at $\omega = -2\omega_l$. Hence, $U_{m,l}(\omega)$, the spectrum of the filtered signal $v_{m,l}(t)$, would be:

$$U_{m,l}(\omega) = H_{m,l}(\omega+\omega_l)S_l(\omega)e^{-j(\omega+\omega_l)\tau_m} + E_{mf}(\omega+\omega_l) \ , \tag{2.12}$$

in which $E_{mf}(\omega+\omega_l)$ is the noise component after passing through the demodulator. Under a quite general scenario, (to be discussed in the sequel), we can approximate (2.12) by the following equation:

$$U_{m,l}(\omega) \approx H_m(\omega_l)S_l(\omega)e^{-j\omega_l\tau_m} + E_{mf}(\omega+\omega_l) \ , \tag{2.13}$$

which assumes the time domain equivalent expression:

$$u_m(t) = H(\omega_l)s_l(t)e^{-j\omega_l\tau_m} + e_{mf}(t) \ , \tag{2.14}$$

where $e_{mf}(t)$ stands for the time domain version of the corresponding term $E_{mf}(\omega+\omega_l)$. We also assume that the channel response $H_{m,l}(\omega) \approx H(\omega_l)$ which means that the channel response at each frequency ω_l is similar for all the M elements of the

array.

If we assume that the support bandwidth of $s_l(t)$, $B_l \ll \omega_l$, then as the frequency $|\omega|$ increases, $S_l(\omega)$ decreases rapidly and hence the approximation in (2.13) follows. In this scenario the bandwidth of the low-pass filter equals the support bandwidth of the signal $s_l(t)$, B_l. Under the above scenario, the contribution of the signal on the output $U_{m,l}(\omega)$ is approximately zero if $\omega > B_l$[1].

Another interpretation of the first scenario is that the signal $s(t)$ does not vary over the array ([31]), which means:

$$s(t) \cong s(t+\tau_m) \text{ which, in the worst case, is : } s(t) \cong s(t+\tau_M) \ . \tag{2.15}$$

In the frequency domain this assumption is translated into:

$$S(\omega) \cong S(\omega)e^{j\omega\tau_M} \ , \tag{2.16}$$

which might be justified if the support bandwidth of $s(t)$, $\mathbf{B} \ll \omega_l$, i.e., $S(\omega)$ dies quickly for $\omega > \mathbf{B}$. This interpretation is frequently referred to the *signal narrow-band assumption*. Note that in the case of Uniform Linear Arrays, τ_m=$(m-1)d\sin(\Theta)/c$. If the frequency of the *standard ULA array* (in which $d/\lambda = 1/2$) is ω_{std}, then $\omega_{\tau_M} = (M-1)\pi\sin(\Theta)\omega/\omega_{std}$.

2. DOA Solutions and *a priori* Distribution of DOA

The solutions adopted in the array processing literature are mainly based on the Bayesian approach. For instance when calculating the Maximum Likelihood Estimate

---

[1]Equation (2.13) can also be achieved from (2.12) under another set of assumptions. If the sensor elements are narrow-band around $\omega = \omega_l$, then $|H_m(\omega+\omega_l)|$ goes quickly to zero as $|\omega|$ increases. Therefore, if the frequency response of the sensor element around ω_l is flat, then we can still achieve (2.13) if $s_l(t)$ varies within the bandwidth of the sensors $\mathbf{B}_{wideband}$. The bandwidth of the low-pass filter in this case matches the bandwidth of the sensor elements $\mathbf{B}_{wideband}$.

(MLE), it is customary to consider a uniform *a priori* distribution for the parameter $q = \sin(\theta)$ rather than θ *per se*. This assumption not only makes the mathematical derivations more convenient, but only paves the way of utilizing analogous results to array processing problems (for instance, adopting the frequency estimation approaches to spatial processing). We can account for this change of variable and *a priori* assumption and express the distribution of the angles θ as:

$$p_\theta(\theta) = \frac{\cos\theta}{q_{max} - q_{min}} \ , \qquad \sin^{-1}(q_{min}) \leq \theta \leq \sin^{-1}(q_{max}) \ , \tag{2.17}$$

where we considered a uniform *a priori* distribution for q over $[q_{min}, q_{max}]$ and $\theta \in [-\pi/2, \pi/2]$. Then one can construct an estimate similar to a *Maximum A Posteriori* (MAP) estimate to amount for the effect on the *a priori* knowledge.

It is worth noting that we still do not know the exact $p_\theta(\theta)$, but wish to compensate the uniform *a priori* assumption on the lumped variable $q = \sin(\theta)$, that are generally considered for derivation convenience. As we consider all-angle estimates throughout this work, Equation (2.17) simplifies to

$$p_\theta(\theta) = \frac{\cos\theta}{2} \ . \tag{2.18}$$

This assumption implies that the DOA estimates in the endfire region are less likely than the broadside of the array. Furthermore, the fact that the *Rayleigh resolution* is worse in the endfire of the array, makes the estimates in this region even more unfavorable. It is however a known problem [32, 33] and there are several methods in the literature which suggest adjusting the element gains across the array to contain this phenomenon (e.g., Hansen-Woodyard procedure [9]).

3. Ambiguities

As per aforementioned remarks, the maximum alias-free frequency of operation for an *all-angle* narrowband uniform linear array equals $\omega_{std} = \pi c/d$ or the *standard frequency* of the array. Increasing the frequency of operation beyond the *standard frequency* results in *rank-one* ambiguity of the steering vector $Q_l(\theta)$, where two distinct transmitters located at different directions may produce the same *array manifold* (i.e., *array manifold crossing*).

It is important to differentiate between two commonly used notions of ambiguity in the array processing literature. The first one being the manifold ambiguity which is discussed above. The second notion addresses the processing algorithms which apply to nontrivially unambiguous problems but can create ambiguity (for instance due to coherency of the signals or the proximity of the transmitters). These ambiguities may be resolved by some other techniques.

Throughout this work, we consider the former notion of ambiguity, and we try to resolve the spatial aliasing using several subbands. If we set the first subband frequency $\omega_1 = \omega_{Std}$, then except this subband, all of the transmission spectrum is beyond the alias-free range of the array. In general, we can have $\omega_1 > \omega_{Std}$, where there is no all-angle alias-free subband or we can set $\omega_1 < \omega_{Std}$, where some or all of the subbands are alias-free for all directions. Both of these scenarios can be incorporated in the model, however for mathematical convenience in developing the algorithm, $\omega_1 = \omega_{Std}$ is considered.

In the next chapter, the problems of DOA and signal estimation are discussed when the steering matrix is folding (or crossing).

CHAPTER III

WIDEBAND MLE-BASED DOA ESTIMATION IN ULAS WITH INORDINATE SPACING USING A SUBBAND HOPPING APPROACH *

A. MLE-based Algorithm

Let us assume that the outputs of the sensors are the time functions $u_m(t)$, $m \in \{1, 2, \ldots, M\}$. We can represent them by vectors $u_l(n)$, after *appropriately* pre-processing and sampling the outputs regularly at arbitrary time instances $n = n_i$, $i \in \{1, 2, \ldots, N\}$, $n_{i+1} - n_i \equiv \Delta n \leq T_h/N \equiv 1/2B$. From this point onward and considering the reservations that are discussed in Section II, we drop the continuous time variable t and use the sampled version n.

Based on assumptions on the source signals, two different models for MLE of the arrival angles could be considered. In both models however, the noise is assumed to be Gaussian, with zero mean and spatially and temporally white, i.e.,

$$E\{e(n)e^H(m)\} = \sigma^2 I \delta_{m,n} \ , \tag{3.1}$$

where $\delta_{m,n}$ is the *Kronecker Delta* function.

One approach is to treat the input signals $\{s(n)\}_{n=1}^N$ as non-random. In other words, we can assume that the signal sequence is frozen in all realizations of the random data $\{u(n)\}_{n=1}^N$. Hence, for each source, aside from the DOA (and probably the noise variance), there are N unknown parameters that need to be estimated

* Major part of this section is excerpted from [34], under blanket permission ©`www.springeronline.com`, and from "Incoherent MLE of array antennas with inordinate spacing using subband hopping approach" [35], ©2006 IEEE with permission.

from N observations. This model is often called *deterministic* or *conditional* model and the MLE solution is called *Deterministic ML* (DML) or *Conditional ML* (CML) respectively.

The second model is the *unconditional* or often-called *stochastic* model, in which we assume that the source signal sequence, $\{s(n)\}_{n=1}^{N}$, is a sample set from a stationary, temporally white complex Gaussian process with zero mean and nonsingular covariance matrix

$$\begin{aligned} E\{s(n)s^H(m)\} &= P\delta_{m,n} \qquad |P| \neq 0 \ , \\ E\{s(n)s^T(m)\} &= 0 \qquad\qquad \forall\ n,m \ , \end{aligned} \tag{3.2}$$

where $|.|$ denotes the determinant operation, and P is the covariance matrix, which along with DOA (and probably the noise variance) needs to be calculated, rather than the individual values at each realization in the conditional model. Therefore under this model, fewer number of parameters are required to be estimated. The MLE solution under this assumption is called *Stochastic ML* (SML) or *Unconditional ML* (UML), respectively.

Under the *conditional* case, the received vectors have the following distributional characteristic:

$$u_l^c(n) \propto \mathcal{N}(Q_l(\theta)s_l(n), \sigma^2 I) \ , \tag{3.3}$$

while under the *unconditional* mode, the outputs, u_l^u, are assumed to have a Gaussian distribution with zero mean:

$$u_l^u(n) \propto \mathcal{N}(0, R) \ , \tag{3.4}$$

where:

$$\begin{aligned} R = E\{u_u(n)u_u^H(n)\} &= Q_l(\theta)E\{s_l(n)s_l(n)^H\}Q_l(\theta)^H + E\{e(n)e^H(n)\} \\ &= Q_l(\theta)P_lQ_l(\theta)^H + \sigma^2 I \ . \end{aligned}$$

Obviously the maximum likelihood estimates for these two models result in different algorithms, nonetheless, unless there is information regarding a specific *a priori* feature regarding the transmitted signals, conditional and unconditional models are oftentimes used on the same data set, and although the underlying models are different, they provide satisfactory results in estimating θ.

In [36], it is shown that the Cramér-Rao bound under the unconditional model is achievable and is smaller than or equal to that of the conditional model (note that as N increases, the number of unknowns also proportionally increases, which makes the MLE inconsistent under the conditional model).

The DML approach is perhaps the most natural technique to use in the applications, where only a small number of snapshots is available. Unless explicitly mentioned in this work, the general approach adopted herein is based on the *conditional* model.

Given the aforementioned assumptions, the column vector of the received signal, $u_l(n)$, is circularly symmetric and temporally white Gaussian random process with mean $s_l(n)\ Q_l(\theta)$ and covariance $\sigma_l^2 I$. The joint probability density function of the sampled data of one source impinging on the array of M elements at the l^{th} frequency subband can be expressed as

$$J_0(\theta_l, s_l(n), \sigma_l) = \frac{1}{(\pi\sigma_l^2)^M} e^{-\|u_l(n) - \ Q_l(\theta)\ s_l(n)\|^2/\sigma_l^2} \ . \tag{3.5}$$

Assuming the measurements are independant and incorporating all the observations

(N), from subband l, the *likelihood* function is given by

$$J_1(\theta_l, s_l(n), \sigma_l) = \prod_{n=1}^{N} \frac{1}{(\pi\sigma_l^2)^M} e^{-\|u_l(n) - \ Q_l(\theta)\ s_l(n)\|^2/\sigma_l^2} \ , \tag{3.6}$$

which further simplifies to the well-known *nonlinear regression model*,

$$J_2(\theta_l, s_l(n)) = \sum_{n=1}^{N} \|u_l(n) - \ Q_l(\theta)\ s_l(n)\|^2 \ . \tag{3.7}$$

Minimizing J_2 results in the ML estimate. This is a multiple parameter estimation problem. We first assume that the parameter θ is fixed and minimize J_2 with respect to $s_l(n)$, solving for the lowest Euclidean norm results in the estimate

$$\hat{s}_l(n) = Q_l^{\dagger}(\theta) u_l(n) \ , \tag{3.8}$$

where $Q_l^{\dagger}(\theta)$ is the Moore-Penrose pseudoinverse of $Q_l(\theta)$, which for this vector simplifies to $Q_l(\theta)^T / \ \| \ Q_l(\theta) \ \|^2$. Plugging this estimate into (3.7) and minimizing with respect to θ, we obtain:

$$J_3(\theta_l) = \sum_{n=1}^{N} \left\| u_l(n) - \ Q_l(\theta)\ Q_l^{\dagger}(\theta) u_l(n) \right\|^2 \ . \tag{3.9}$$

Hence, the ML estimate is obtained by maximizing:

$$J_4(\theta_l) = \sum_{n=1}^{N} \left\| \ Q_l(\theta)\ Q_l^{\dagger}(\theta)\ u_l(n) \right\|^2 \ . \tag{3.10}$$

The above equation can be equivalently simplified to

$$J_5(\theta_l) = Tr(Q_l(\theta)\ Q_l^T(\theta)\ \hat{R}_l) \ , \tag{3.11}$$

in which $\hat{R}$ is the sample covariance matrix of the received signals at frequency subband l. Hence, the ML estimate would be

$$\hat{\theta}_l = arg \left\{ \max_{\theta} \ Tr \ (Q_l(\theta)\ Q_l^T(\theta)\ \hat{R}_l) \right\} \ . \tag{3.12}$$

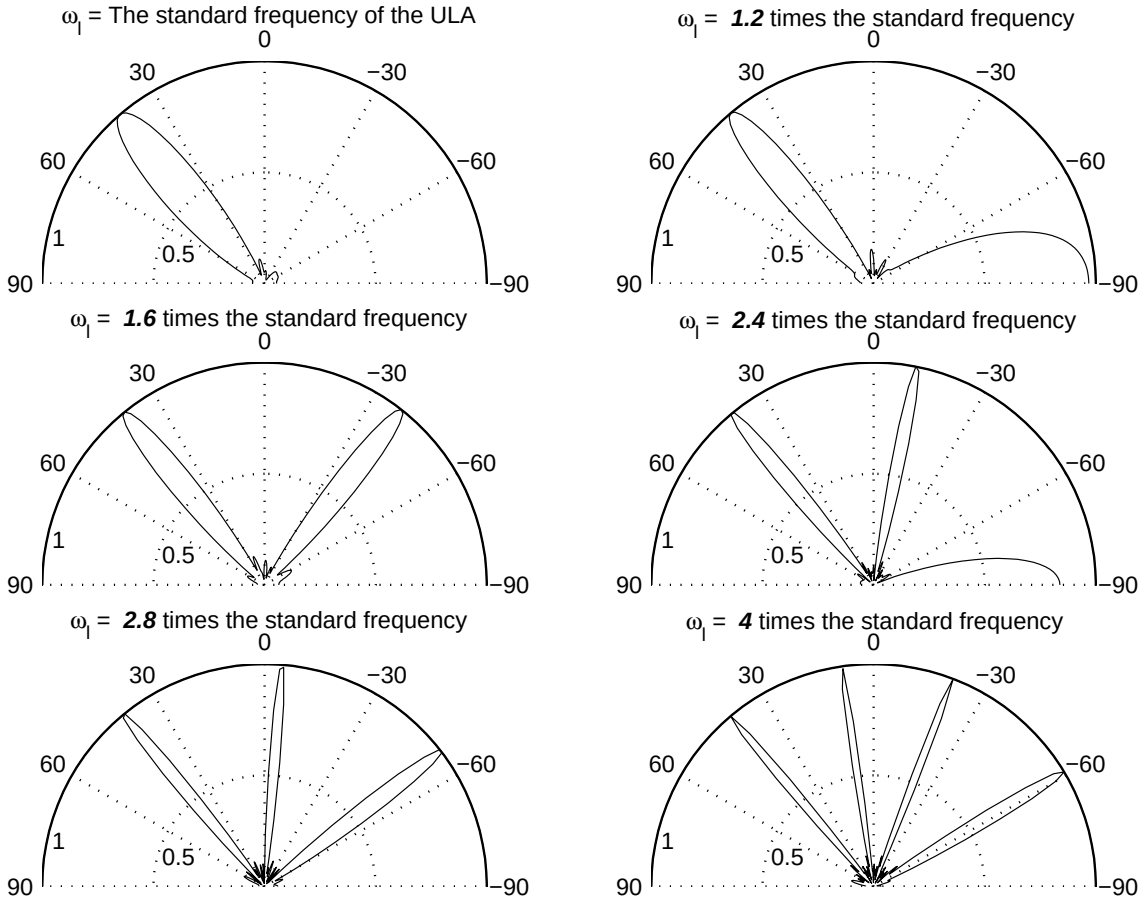

Fig. 3. Normalized DOA estimate using $N = 4$ snapshots at each frequency subband of a 7 element array antenna with SNR=3dB per each subband, when the source is 40 degrees relative to the broadside of the array.

Figure 3 shows independent MLE of an array at each subband, when the wide-band source is fixed at a certain angle. Within the adopted mathematical formalism, we can visually verify that the inordinate spacing of the antenna elements creates *grating lobes*, which results in multiple angle estimates. The remaining problem is to sift the true direction of arrival from the spurious estimates or maxima in (3.12) and then estimate the transmit signals at each subband.

B. The Number and the Loci of the Grating Lobes

The accuracy of DOA estimates in ULA increases as the aperture size of the array increases [18], however as the element spacing increases the spurious (grating) lobes move to the visible region. In a similar vein, and given the reciprocality of this error, two distinct angles would lead to the same steering vector.

There are inherent ambiguities with linear arrays for sources which are symmetrical with respect to the broadside of the array, i.e., when $\theta_2 = 180^\circ - \theta_1$. Such ambiguities cannot be avoided [37, 38] and for all practical purposes, we restrict the scanning angle to $[-90^\circ, 90^\circ]$. If the true angle of the source is at θ, the loci of the grating lobes can be calculated as

$$\theta_g = \sin^{-1}\left(\sin\theta - \frac{\kappa}{\zeta}\right) , \tag{3.13}$$

where $\zeta = d/\lambda$ and $\kappa = 1, 2, 3, \ldots$ (for all integers which are possible). Equation (3.13) is highly nonlinear.

Figure 4 shows the onset of the grating lobes (i.e., $\kappa = 1$). The grating lobe remains out of the visible range of the array, $[-90^\circ, 90^\circ]$, if $\zeta \leq 0.5$. Figure 5 illustrates the relationships between the number of the grating lobes κ, the source angle θ and the interelement spacing per wavelength ζ.

The total number of the grating lobes κ at a subband with $\zeta = \zeta_l$ can be expressed as

$$\left\{\kappa = 1, 2, 3, \ldots \;\middle|\; 0 < \frac{\kappa}{\zeta_l} \leq 2\right\} . \tag{3.14}$$

In view of (3.13), to ensure that the estimates of the grating lobe angles do not construct a maximum after the histogram combining, we should have $\theta_{g1}|_{\zeta=\zeta_p} \neq$

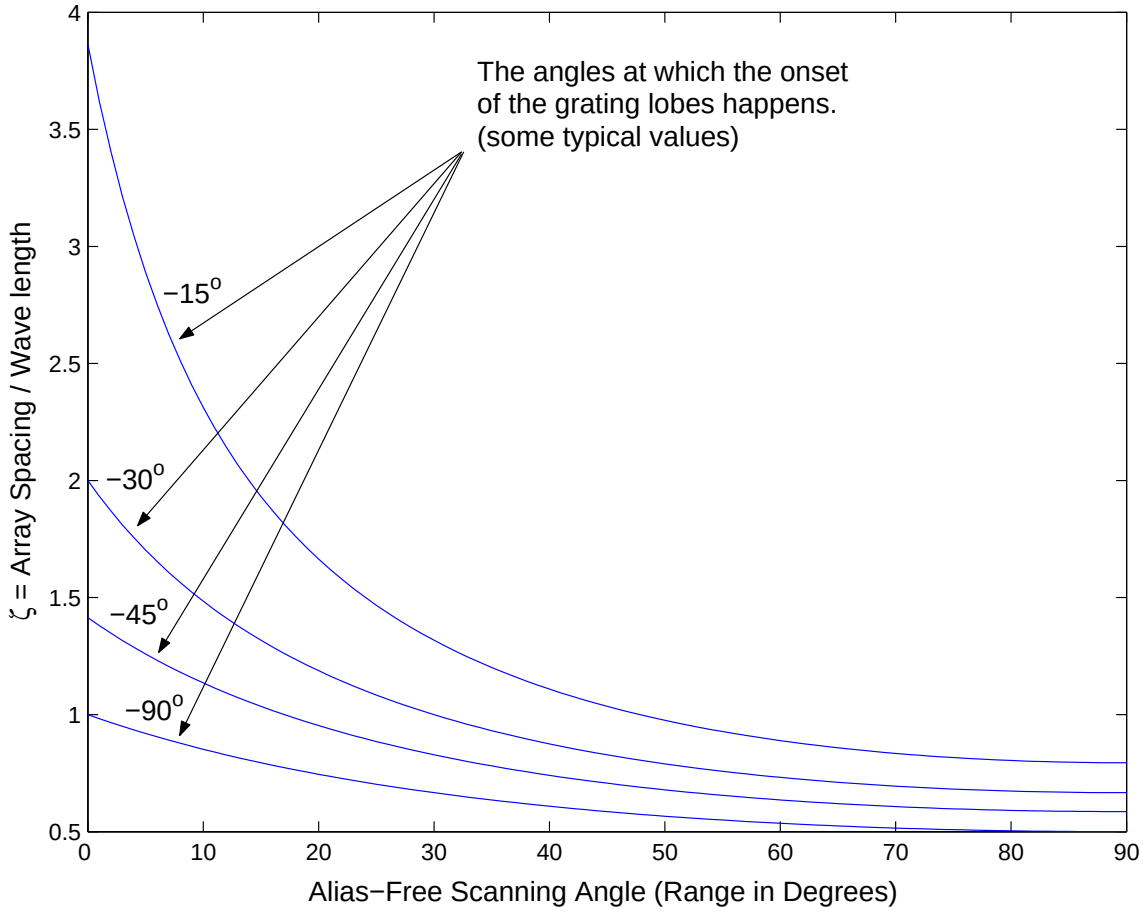

Fig. 4. The onset of the grating lobes.

$\theta_{g2}|_{\zeta=\zeta_q}$ for all subbands $p \neq q$, hence:

$$\frac{\kappa_1}{\zeta_p} \neq \frac{\kappa_2}{\zeta_q} \ , \tag{3.15}$$

for any integers κ_1 and κ_2 ($\kappa_1 \neq \kappa_2$), which are constrained by (3.14). Hence, the maximum possible number of aliasing angles at subband frequency l is:

$$\hat{\kappa}_{max} = \lfloor 2\zeta_l \rfloor \ . \tag{3.16}$$

An extension of the methodology which is addressed in this section has been adopted to two–dimensional arrays. This is discussed in Appendix B.

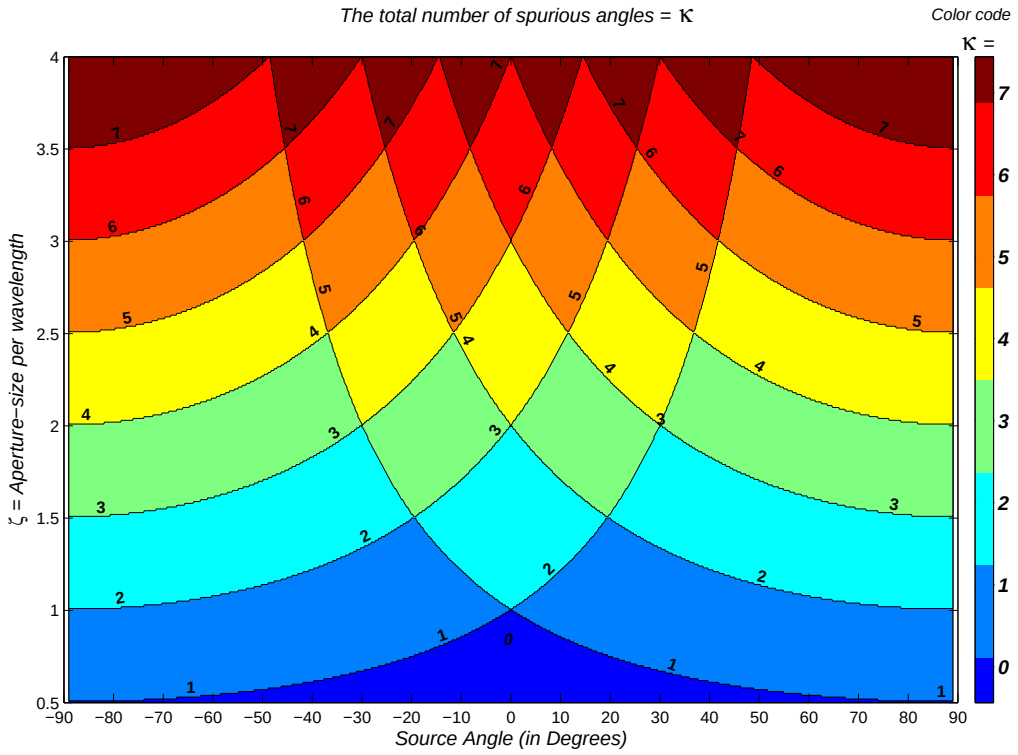

Fig. 5. The nonlinear relationship between the number of the aliasing angles, the true angle and the aperture size.

Note that the step of finding a good set of frequency subbands for subband hopping to satisfy (3.15) poses no realtime computational burden on the array processor.

C. Resolving the Aliasing by Combining the Estimates

As it can be seen from Figure 3, at higher frequencies, despite the correct estimates at the correct angle and given the constraints in (3.14) and (3.15), the grating lobes appear at different angles in each sub-band. One obvious approach is to consider unknown *Joint Random Plus Aliasing Noise* distribution and use non-parametric density estimators such as *histogram* or *Kernel or Parzen Density Estimators (KDE)*[39] for DOA estimation. Let us assume that P_{θ_l} is the probability that the likelihood of

the observation vector $J_5(\theta_l)$ in (3.11), drawn from the underlying distribution $p(\theta_l)$, falls in a given region $\mathcal{R}$ (e.g., DOA vicinity) of the sample space $\mathbf{\Omega}$. Note that we are eventually looking for the dominant peaks of the likelihood function. $\mathcal{R}$ is assumed a surface of two dimensions, the first (horizontal) dimension is an angular interval ($[\theta_1, \theta_2]$), and the second (vertical) dimension is the amplitude interval for the likelihood function. Both of the dimensions are associated with the angular and amplitude granularity of the array processor. The index, l, refers to one of the L subbands. Since in non-coherent (blind) combining, we do not differentiate among the underlying distributions in different subbands, we drop the index l

$$P_{\theta_l} \approx P_\theta \qquad \text{and} \qquad p_{(\theta_l)} \approx p_{(\theta)} \ . \tag{3.17}$$

Then we have

$$P_\theta = \int_{\mathcal{R}} p(\theta')d\theta' \ . \tag{3.18}$$

One observation vector is drawn from each of L subbands according to (3.11) from the underlying (pseudo) distribution. The probability that the likelihood values of k of these L vectors falls in $\mathcal{R}$ is given by binomial distribution

$$P(k) = \binom{L}{k} P_\theta^k (1 - P_\theta)^{L-k} \ . \tag{3.19}$$

From the properties of binomial distribution, it is well known that

$$E[\frac{k}{L}] = P_\theta \qquad \text{and} \qquad Var[\frac{k}{L}] = \frac{P_\theta(1 - P_\theta)}{L} \ . \tag{3.20}$$

Therefore, as the number of subbands increases (i.e., $L \to \infty$), the variance becomes smaller, and we expect a sharper distribution, and a good probability P_θ can be obtained from the mean fraction of the likelihoods, i.e., peaks in (3.11), at which

$P_\theta \simeq k/L$. If we approximate $p(\theta)$ as constant within $\mathcal{R}$

$$P_\theta = \int_{\mathcal{R}} p(\theta')\ d\theta' \simeq p(\theta)\mathcal{S}\ , \tag{3.21}$$

where $\mathcal{S} = \triangle_J \times \triangle_\theta$ is the *volume* of $\mathcal{R}$ and θ is some point lying inside $\mathcal{R}$. $\triangle_\theta$ is the angular observation width and $\triangle_J$ is the quantized amplitude to a desirable degree. We can write the intuitive result

$$p(\theta) \simeq \frac{k}{L\ \triangle_J \times \triangle_\theta}\ . \tag{3.22}$$

Equation (3.22) is the familiar histogram. The above estimate becomes more accurate as the number of observations from each subband, L, increases and as the volume $\mathcal{S}$ decreases. As it is intuitively obvious, there is a compromise between the number of frequency bands and the granularity of DOA estimation. DOA is then simply the largest statistical *mode* (i.e., the most likely value) among all angle intervals of all the surfaces $\mathcal{S}$, or

$$\hat{\theta}_l = arg\left\{\max_\theta\ mode\ (p(\theta)\ |\mathcal{S}_{\triangle_J,\triangle_\theta})\right\}\ , \tag{3.23}$$

where $\theta \in [\theta_1, \theta_2]$. In the limit of an infinite number of subbands ($L \to \infty$), it is expected that the performance of the proposed estimator to improve, as $\mathcal{R}$ can become smaller (i.e., better accuracy), while ensuring that it still contains an ever increasing number of points. A more elaborate density estimation approach is the Parzen density estimator. Unlike parametric or finite-mixture density estimation approaches, where only sufficient statistics and mixing weights are required in estimation, Parzen density estimation employs the full data sample in defining density estimates for observations. Nonetheless, practical Parzen density estimation does not tend to avoid cumbersome calculations in the above histogram implementation. Perhaps an alternative approach

is to average the subband estimates at different frequencies in view of (3.11)

$$J_{Ave}(\theta) = \frac{1}{L} \sum_{l=1}^{L} \{Tr(Q_l(\theta)\ Q_l^{\dagger}(\theta)\ \hat{R}_l)\}\ , \tag{3.24}$$

and then use the above for MLE, i.e.,

$$\hat{\theta}_l = arg\,\{\max_{\theta}\ J_{Ave}(\theta)\}\ . \tag{3.25}$$

In fact (3.25) suggests a computationally less demanding estimate when we substitute the statistical *mode* at each angle interval with the statistical *mean*. Notice that due to the Law of Large Numbers (LLN), (3.25) converges to the true mean or the true DOA. If we use this method and use the estimates at subbands as samples, the grating lobes would average out while the true angle estimates add up consistently. Figure 6 shows the resulting estimate of a 7-element array antenna using the histogram approach under the following condition: $M = 7$, $\theta = 40°$, SNR = 3 dB, $L = 16$, $N = 4$, $\omega_1 = \omega_{std}$, $\delta = 1/T_h = 0.2\omega_{std}$ and $\omega_i = \omega_{i-1} + \delta$. The reduced impact of the aliasing lobes and a sharper angle estimate are among the advantages of this method. The off-line calculations described in Section B help avoid the grating lobes at different frequencies occurring at the same spurious angles, which would adversely impact the performance of this estimator.

The proposed wideband angle and signal estimation algorithm can be simply summarized as follows:

1. Off-line check of the subband frequencies to avoid the overlapping of the spurious angles at subbands according to (3.14) and (3.15).

2. ML estimate at each subband, i.e., (3.12).

3. Normalize the estimates at each subband.

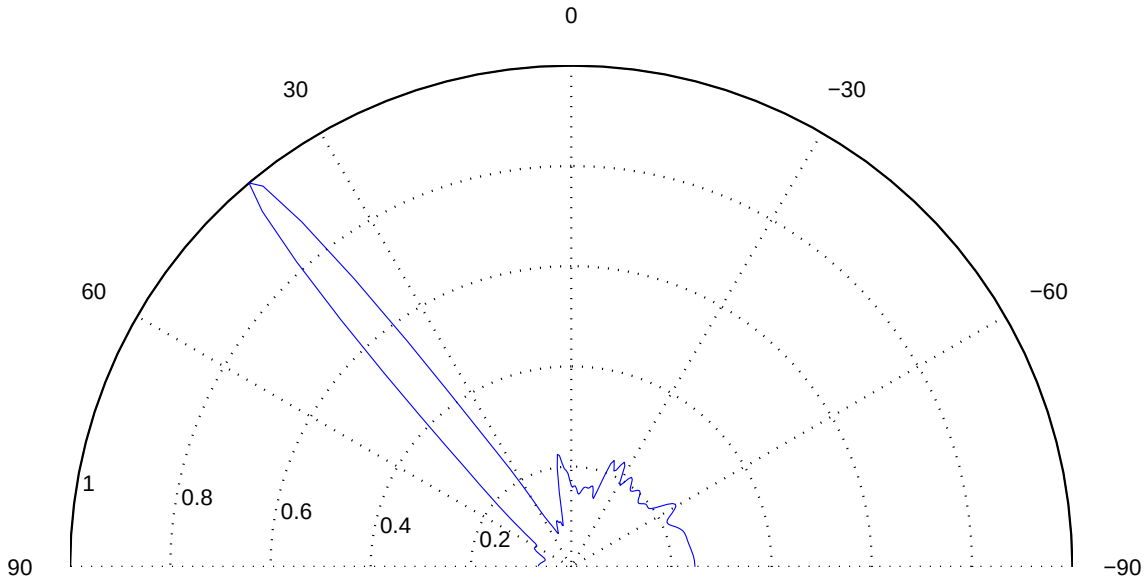

Fig. 6. MLE-based estimate resulting from combining the estimates at all subbands.

4. Apply (3.23) or (3.24) and (3.25) to estimate θ.

5. Use (3.8) to calculate the signals at each subband and apply the appropriate demodulator.

Other faster optimal or suboptimal approaches can replace the ML search step.

D. Multiple Access Using Subband Hopping

Consider K disjoint subband sets $\Omega_1, \Omega_2, \ldots, \Omega_K$ in which $\Omega_k = \{\omega_{k1}, \omega_{k2} \ldots \omega_{kL}\}$. Hence, in total, we have $K \times L$ frequency bands, each band having (without loss of generality) the same spectral support of B Hz for data signals. The only restriction applied here is the subband frequency separation among all of the $K \times L$ subbands which is discussed in Appendix C. We assume that $\delta = \min(\omega_{ap} - \omega_{bq}) = 1/T_h$, where ω_{ap} is the p^{th} subband frequency of Ω_a subband set and ω_{bq} assumes a similar defini-

tion. The receiver chooses one of the sets, known to the transmitter for transmission at each hop. Therefore, at any given time, different sources transmit different subbands and thus interference is avoided. Similar to spread spectrum frequency hopping, this methodology inherently addresses the problem of source association, near-far and multipath problems under the weak condition that the subband frequencies (i.e., ω_{kl}) at each set, Ω_k, are adequately separated. The rather stronger assumption in this scheme is the *narrowband signal assumption*, which requires that the signal $s_l(t)$ (i.e., the transmit data signal at subband l) does not vary over the array length or in the worst case, $s(t) \cong s(t + \tau_M)$, where $\tau_M = (M-1)d \sin\theta/c$ and c is the propagation velocity. This interprets in the frequency domain as $S(\omega_l) \cong S(\omega_l)e^{j\omega\tau_M}$. Therefore, one can ensure the narrowband assumption, if $B \ll \omega_l$, so that $S(\omega)$ fades out quickly when $\omega > B$. It is worth noting that we did not restrict the specific baseband signal format to address the narrowband signal assumption, and only the constraint on the spectral support.

E. Relationship between ML–based Algorithm and Conventional Beamforming

In this section, we address the relationship between the conventional beamforming and the *Maximum Likelihood Estimate* under *deterministic* models.

We first review the conventional beamforming. If the array manifold is known, one can steer the array electronically to a specific direction. A weight vector $\mathbf{W}_l$ and a summer (adder) can be used for each subband l to linearly combine the output signals to form a single output (i.e., superposition of the outputs). Referring to Figure 7, if we assume that $\mathbf{u}_l(n)$ is wide-sense stationary, in the *noiseless* case, the average output power of $\varphi_l(t)$ is:

$$P_{\varphi_l} = E(\varphi_l^2(n)) = \mathbf{W}_l^H \; R_{u_l} \; \mathbf{W}_l \tag{3.26}$$

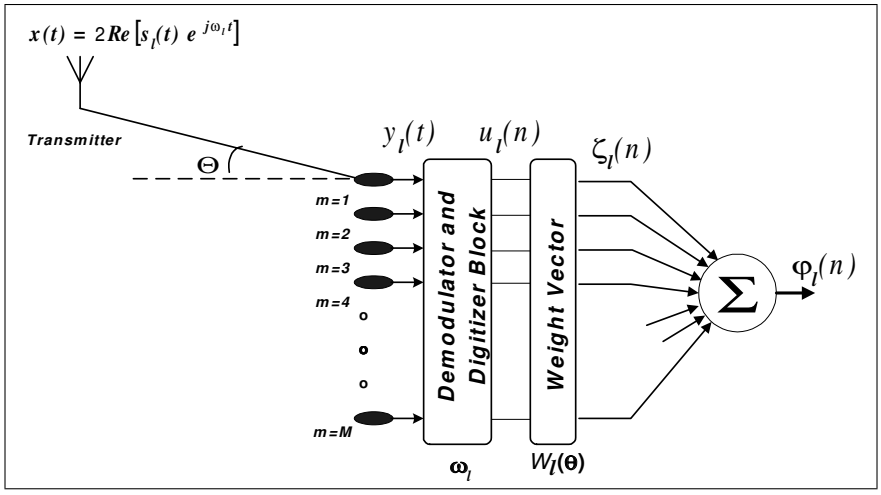

Fig. 7. Spatial weighting vector at frequency subband l.

If we further assume that $\mathbf{u}_l(n)$ is spatially white or $R_{u_l} = I$, then we can write:

$$P_{\varphi_l} = W_l^H \; W_l \tag{3.27}$$

Steering toward a direction θ_0 corresponds to minimizing the power P_{φ_l} at all angles, except the *look direction*, θ_0, so:

$$\begin{cases} \min_W \;\; P_{\varphi_l} = W_l(\theta)^H \; W_l(\theta) \\ \\ \text{subject to} \;\; W_l(\theta)^H \; Q_l(\theta) = 1 \end{cases} \tag{3.28}$$

Utilizing the *Lagrange Multipliers* approach:

$$\begin{aligned}
\Gamma(W_l,\lambda) &= \frac{1}{2}\big[W_l^H(\theta)\ W_l(\theta)\big] + \lambda\big[1 - W_l^H(\theta)\ Q_l(\theta)\big]\ . \\
\frac{\partial\ \Gamma(W_l,\lambda)}{\partial\ W_l^H(\theta)} = 0 &\implies W_l(\theta) - \lambda Q_l(\theta) = 0\ , \\
&\implies W_l(\theta) = \lambda\ Q_l(\theta)\ . \\
\frac{\partial\ \Gamma(W_l,\lambda)}{\partial\ \lambda} = 0 &\implies 1\ -\ W_l^H(\theta)Q_l(\theta) =\ 0\ , \\
W_l(\theta) &= \frac{Q_l(\theta)}{Q_l^H(\theta)Q_l(\theta)}\ =\ \frac{Q_l(\theta)}{M}\ ,
\end{aligned} \tag{3.29}$$

using the fact that:

$$\|Q_l(\theta)\|^2 = Q_l^H(\theta)Q_l(\theta) = M\ . \tag{3.30}$$

This implementation is analogous to the design of Finite Impulse Response (FIR) filters in which the weights of a filter are chosen to minimize the filter output power under the constraint that the filter response for a given frequency, e.g., f_0, is fixed. Because of this similarity, the beamforming method is often called the *Delay-and-Sum* method.

We also note that in the present derivation, the weighings are obtained independently from the data signal statistics as we *blindly* assumed that $\mathbf{u}_l(n)$ was spatially white. From this perspective, this method might be interpreted as a *nonparametric* method [31].

If the beamforming weighting method in Equation (3.29) is used, the actual *noiseless* output power would be:

$$\hat{P} = \frac{Q_l^H(\theta)\hat{R}Q_l(\theta)}{M^2}\ , \tag{3.31}$$

where

$$\hat{R}_l = \frac{1}{N}\sum_{n=1}^{N} u_l(n)u_l^H(n)\ , \tag{3.32}$$

and we used the sample covariance matrix of the received signals, $\hat{R}$, as the signal autocorrelation R is normally unknown.

The DOA estimates are then the locations of the peaks of (3.31), however juxtaposing this estimate with the MLE Equation (3.11) immediately indicates that:

$$Tr\big[Q_l(\theta)\ Q_l^T(\theta)\ \hat{R}_l)\big] \propto \frac{Q_l^H(\theta)\ \hat{R}_l\ Q_l(\theta)}{Q_l^H(\theta)\ Q_l(\theta)} \propto Q_l^H(\theta)\ \hat{R}_l\ Q_l(\theta)\ . \tag{3.33}$$

Hence, maximizing the beamformer spectrum is equivalent to MLE under the deterministic signal model. The above criterion holds if $\mathbf{u}_l(n)$ is spatially white, i.e., each antenna element has omnidirectional pattern. In fact, in [40], it is shown that the above criterion also holds under the *stochastic signal model*, where only a single transmitter impinges on the array. Although we do not address the stochastic model in this dissertation, the single transmitter assumption still holds for our setup with subband hopping approach.

CHAPTER IV

WIDEBAND SUBSPACE-BASED DOA ESTIMATION IN ULAS WITH INORDINATE SPACING USING A SUBBAND HOPPING APPROACH *

A. Subspace-based Algorithm

The sampled spatial covariance of the received vector at frequency l is:

$$\begin{aligned} \mathbf{R}_l &= E\{u_l(n)u_l^H(n)\} \\ &= Q_l(\theta)E\{s_l(n)s_l^H(n)\}Q_l^H(\theta) + E\{e_l(n)e_l^H(n)\} \\ &= Q_l(\theta)\mathbf{P}_l Q_l^H(\theta) + \sigma_l^2 I \ , \end{aligned} \tag{4.1}$$

where $u_l(n)$ is the column submatrix of the received signal defined in Sections II and III, and $\mathbf{P}_l$ is the data signal covariance matrix. The conventional MUSIC method, splits the eigenvectors of $\mathbf{R}_l$ into two orthogonal subspaces, namely the signal space (corresponding to the $\hat{K}$ largest eigenvalues) and the noise space (corresponding to the rest of $M - \hat{K}$ eigenvalues). This requires the following two assumptions that are discussed later:

Assumption A.1. *The rank of the signal space is known. Despite our assumption that we have just one wideband source impinging on the array, $\hat{K}$ is not necessarily one in the presence of aliasing. We investigate how we can identify a good $\hat{K}$ in Section B.*

---

* ©2006 IEEE. Reprinted, with permission, from "A subspace approach for DOA estimation of uniform linear arrays with increased element spacing applicable to wideband transmission" [41].

Assumption A.2. *$Q_l(\theta)\mathbf{P}_l Q_l^H(\theta)$ should be at least of rank $\hat{K}$ ensuring that the nonlinear equation entails the true angle and the aliasing angles (i.e., avoiding the penalty as the result of* order underestimation*).*

Observing the above constraints, (4.1) can be decomposed into (see e.g., [8]):

$$\mathbf{R}_l = \mathbf{U}_{s,l}\Lambda_{s,l}\mathbf{U}_{s,l}^H \ + \ \mathbf{U}_{n,l}\Lambda_{n,l}\mathbf{U}_{n,l}^H = \ \mathbf{U}_l\Lambda_l\mathbf{U}_l^H \tag{4.2}$$

where $\mathbf{U}_{s,l}$ and $\mathbf{U}_{n,l}$ are the signal and the noise eigenvectors, respectively. $\mathbf{U}_l$ is unitary and Λ_l is a diagonal matrix which contains the sorted eigenvalues of $\mathbf{R}_l$. Any vector orthogonal to $\mathbf{Q}_l(\theta)$ is an eigenvector of $\mathbf{R}_l$ with the eigenvalue σ_n^2. Provided that we choose a correct $\hat{K}$, the partitioning would result in $\Lambda_{n,l} = \sigma_n^2 I$. Hence,

$$\mathbf{R}_l = \mathbf{U}_{s,l}\Lambda_{s,l}\mathbf{U}_{s,l}^H \ + \ \sigma_l^2\mathbf{U}_{n,l}\mathbf{U}_{n,l}^H \ . \tag{4.3}$$

Therefore, the eigenvectors of the covariance matrix $\mathbf{R}_l$ belong to either of these two orthogonal subspaces.

It can be simply proved via trigonometric equalities for the calculation of the aliasing angles (or grating lobes) that if θ_l is the aliasing angle of θ_k, then θ_k also is the aliasing angle of θ_l with the same array setup. When spatial aliasing exists, two distinct (aliasing) angles θ_l and θ_k, would produce the same $\mathbf{Q}_l(\theta)$ making the array *ambiguous*. Hence, if one searches through all possible $\mathbf{Q}_l(\theta)$ to find those that are orthogonal to the noise subspace, aliased and true DOA estimates could be determined (given $\hat{K}$)

$$\mathbf{U}_{n,l}^H\mathbf{Q}_l(\theta) = 0, \quad \theta \in \{\theta_1, \ldots, \theta_{\hat{K}}\} \ . \tag{4.4}$$

If $\hat{R}$ is the sample covariance matrix of the received signals,

$$\hat{R}_l = \frac{1}{N}\sum_{n=1}^{N} u_l(n)u_l^H(n) \ , \tag{4.5}$$

then it can be used in the decomposition formula (4.2) to calculate the noise eigenvectors $\hat{\mathbf{U}}_{n,l}$ and the estimate of the orthogonal projector onto the noise subspace, i.e.,

$$\hat{\Pi}_l^{\top} = \hat{\mathbf{U}}_{n,l}\hat{\mathbf{U}}_{n,l}^{H} \ .$$

Hence, finding the DOA's in (4.4) could be alternatively achieved by:

$$J_l(\hat{\theta_0}) = arg\left\{ \max_{\theta} \frac{\mathbf{Q}_l(\theta)\mathbf{Q}_l^H(\theta)}{\mathbf{Q}_l^H(\theta)\hat{\Pi}_l^{\top}\mathbf{Q}_l(\theta)} \right\} \ . \tag{4.6}$$

The orthogonality between $\mathbf{U}_{n,l}$ and $\mathbf{Q}_l(\theta)$ at each frequency bin gives rise to peaks in (4.6) and the $\hat{K}$ largest peaks correspond to the true and the aliasing angles.

B. Resolving the Ambiguity

Knowledge of the number of angles K, a parameter necessary in the decomposition (4.2), represents the key step in the proposed subspace algorithm. Since the sample covariance matrix (4.5) is formed using a finite set of samples, identifying the multiplicity of the smallest similar eigenvalues $M - \hat{K}$ is inaccurate.

Underestimating would risk the desired true angle to appear in the noise space, while the aliasing angles would dominate the signal space. On the other hand, overestimating of the number of the aliasing lobes would result in the mixture of noise and signal subspaces. However, overestimating exhibits less risk as the following algorithm would reduce the impact of the interfusion of noise on the signal subspace, as the number of subbands increases.

Let $J_l(\hat{\theta_0})$ in (4.6) be the estimated angles after deploying the subspace algorithm with $\hat{K} = \hat{\kappa}_{max}$, obtained in (3.16), when the source is arbitrarily at θ_0. The set of angles is likely to consist of the true angle, the aliasing angles and probably the spurious angles due to the noise subspace. Since the source is a wideband transmitter

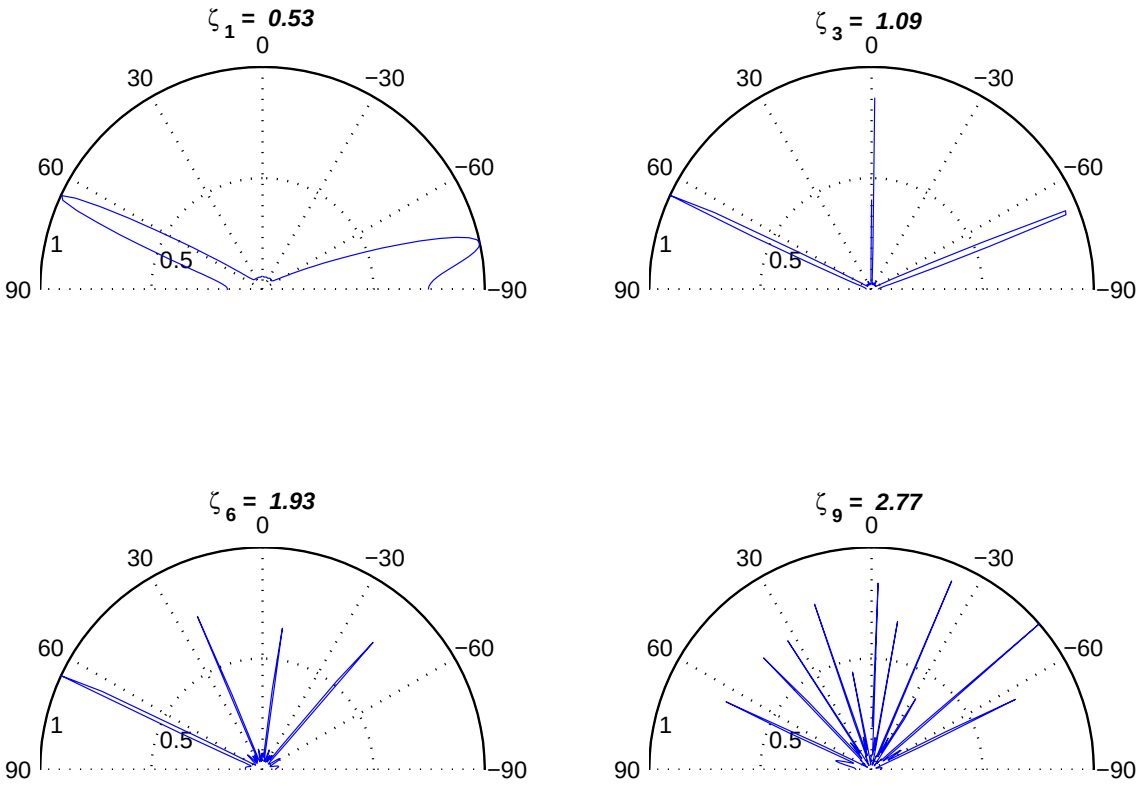

Fig. 8. Subspace estimates at different aperture-size per wavelengths corresponding to different frequency bins, $\zeta_l = d/\lambda_l$, when $\theta_0 = 65°$, $M = 7$, $SNR = 5dB$ and $N = 6$.

with L frequency bands, there are L such estimates: $\mathbf{J}_L = \{J_1(\hat{\theta_0}), J_2(\hat{\theta_0}), \ldots, J_L(\hat{\theta_0})\}$.

Figure 8 shows J_1, J_3, J_6, J_9 angle estimates (at some typical subbands). Note the appearance of the grating lobes or the aliasing angles in the visible range at higher frequencies. Our objective is to find the true direction of arrival θ_0 from the estimates $\mathbf{J}_L$. Since the true angle estimate is likely to exist in all estimates, the subspace processor renders it amenable to similar non-parametric density estimators which were discussed earlier in Section C. In the simplest (*histogram*) form, the resulting

angle estimate would be:

$$\hat{\theta}_0 = \max \ \mathrm{E}\big\{ J_l(\hat{\theta}_0) \big\} \quad , \quad l \in [1 \dots L] \ , \tag{4.7}$$

while observing the assumptions discussed in (3.14) and (3.15).

Figure 9 shows the final result of the source angle estimate. Once the DOA estimate is calculated, we can calculate the transmitted data signals [25]:

$$\hat{s}(n) \quad = \quad Q_l^{\dagger}(\theta) u_l(n) \ , \tag{4.8}$$

where $Q_l^{\dagger}$ is the generalized left inverse of the matrix Q_l (e.g., Moore-Penrose inverse).

Suppose the wideband source is at direction θ_0, then the proposed algorithm may be summarized as follows:

1. Off-line check of the frequency bins to avoid the overlapping of the spurious angles according to (3.14) and (3.15).

2. Collect input signals u_{ml} and calculate the sample covariance matrix at each frequency $\mathbf{R}_l$.

3. Calculate the maximum number of the aliasing angles $\hat{\kappa}_l$ at each frequency bin l.

4. Calculate DOA estimate at each frequency l using (4.6).

5. Normalize the amplitude level of estimates at each estimate .

6. Apply (4.7) to find $\hat{\theta}_0$.

7. Use (3.8) to calculate the transmit signals at each frequency bin [42] or apply appropriate demodulator (e.g., BPSK).

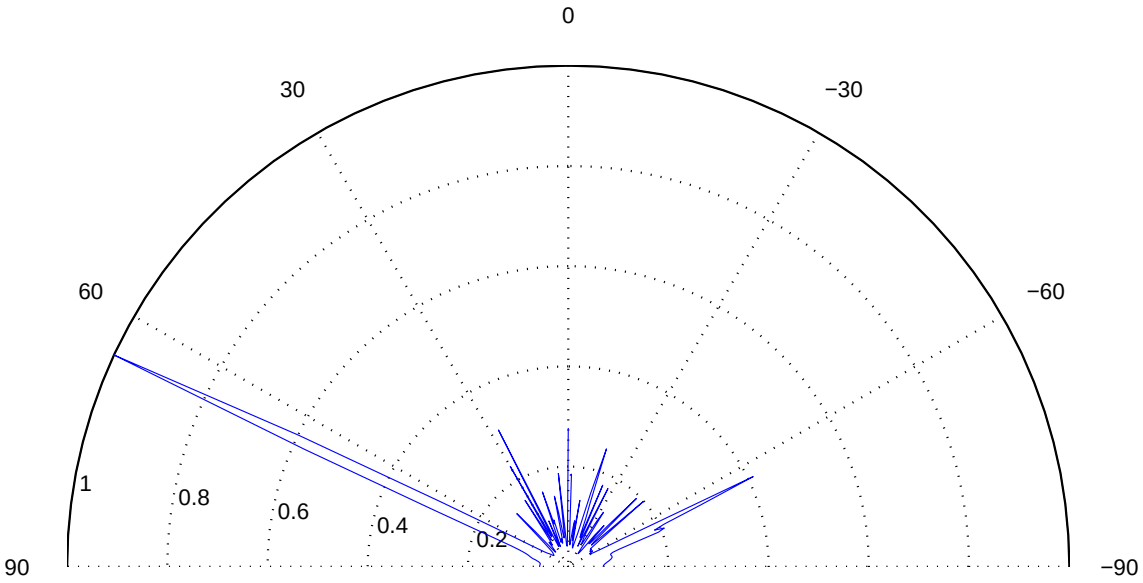

Fig. 9. Final angle estimate when $\theta_0 = 65°$, $M = 7$, $SNR = 5dB$ and $N = 6$, $L = 9$, $\zeta \in \{0.53, 0.81, 1.09, 1.37, 1.65, 1.93, 2.21, 2.49, 2.77\}$.

Despite the underlying derivations and arguments, the implementation of the proposed setup and algorithm is simple and assumes relaxed constraints. The rich wideband spectrum conveniently affords the multiple access deployment.

CHAPTER V

ERROR MAGNITUDES UNDER ALIASING

The mean-square estimation error of a non-random parameter is lower-bounded by the *Cramér-Rao Bound* (CRB). CRB, however, is not a tight bound for certain models, exhibiting e.g., low SNR, finite sample regimes. In these scenarios, this bound leads to overly optimistic estimates of system performance. This prompted the development of alternative bounds over the years, e.g., the Barankin, Ziv-Zakai, and Weiss-Weinstein bounds. The MLE under certain regularity conditions attains asymptotically the minimum variance as given by CRB [8]. However, exact expressions for the bias and variance of the MLE in the non-asymptotic region are still often difficult to compute.

In this section a lower bound on the variance of the estimator under spatial aliasing is presented. As addressed earlier in Section B, the loci and the number of aliasing angles are not available in closed form. The actual number of the aliasing lobes, i.e., $\kappa_{\theta_0} \leq \hat{\kappa}_{max} = \lfloor 2\zeta_l \rfloor$, depends on the source angle at subband frequency l.

The estimators, which are discussed in Sections C and B, perform DOA estimation by data mixtures of different subbands. At subband frequency l, an approximation of the error size using the CRB can be calculated under the multi-source scenario when the number of transmitters is upper-bounded by $\hat{\kappa}_{max}$. Note that this derivation is in regard to just one subband and we do not consider the multi-source implementation which is utilized by the subband-hopping approach of Section D.

First, an error bound is derived when only one subband is used for estimation. It is shown that, as expected, our proposed array processor could not limit the error magnitude in this scenario. In the later part of this section, we derive an error bound when multiple subbands are used in the estimation process.

By using the law of total probability, the *Mean Square Error (MSE)* of the

estimator at the subband frequency l can be expressed as [43]:

$$\text{MSE} = E\Big[(\hat{\theta}-\theta_0)^2\Big] = Pr\Big[\theta_0\Big]\ E\Big[(\hat{\theta}-\theta_0)^2|\theta_0\Big] + \ Pr\Big[\theta_f\Big]\ E\Big[(\hat{\theta}-\theta_0)^2|\theta_f\Big] \tag{5.1}$$

where θ_0 is the true angle, θ_f is any other angle (i.e., false angle), and $\hat{\theta}$ is the estimate. Note that the subscript l, which associates the probabilities and the estimation errors to the subband l, has been intentionally dropped to avoid notational distraction.

The aliasing angles, θ_κ, present major contributions on the overall MSE of the estimator as their amplitudes are similar to that of the true angle. Therefore, we can write the following approximation:

$$Pr\Big[\theta_f\Big]\ E\Big[(\hat{\theta}-\theta_0)^2|\theta_f\Big] \approx \sum_{\kappa=1}^{\kappa_{\theta_0}} Pr\Big[\theta_\kappa\Big]\ \Big[(\theta_\kappa-\theta_0)^2\Big]\ . \tag{5.2}$$

Furthermore by approximating the *local* errors asymptotically to CRB_l in the region close to the true angle, we obtain:

$$E\Big[(\hat{\theta}-\theta_0)^2|\theta_0\Big] \approx \text{CRB}_l\ . \tag{5.3}$$

CRB_l in the above approximation represents the *local* MSE in the asymptotic sense, conditioned on the event that the estimate has actually attained the true angle given an *alias-free* setup. The best local approximate to this bound is achieved when the true angle lobe in the aliasing scenario is simulated by an analogous lobe under alias-free scenario. The lobe width of an alias-free setup is generally wider than the aliased setup. The number of elements of an alias-free *standard* array, M_{af}, with analogous *half power bandwidth* to an aliased array would be:

$$M_{\text{af}} \approx \frac{M\zeta_l}{\zeta_{\text{af}}}\ , \tag{5.4}$$

where $\zeta_{\text{af}} \leq 0.5$ is an arbitrary number which makes M_{af} an integer. M and ζ_l are correspondingly the number of elements and the interelement spacing per wavelength

at subband frequency l of an *aliased* array. In calculating the *half power bandwidth* at subband l, $\Delta\theta_{H_l}$, we used the following approximation for each subband:

$$\Delta\theta_{H_l} \approx 0.891 \frac{\sec\theta_0}{M\zeta_l} \ . \tag{5.5}$$

It can be shown that the above approximation is relatively accurate and has a maximum error of 4% when $M\zeta \geq 5$ in the worst region (i.e., the endfire region) [8, Sec. 2.5]. Therefore, CRB_l can be calculated by plugging the new quantities at CRB for an alias-free array (of size M_{af} and interelement spacing of $\zeta_{\mathrm{af}} \leq 1/2$), which is readily available in the literature (e.g., [8, 44]). Adopting and simplifying the CRB expression which is derived in [44] to our problem, and given the transform (5.4), we obtain:

$$\mathrm{CRB}_l = \frac{\sigma^2}{N(D^H D \odot \hat{P}^T)} \ , \tag{5.6}$$

where

$$D = \frac{\partial Q_l(\theta)}{\partial\theta}\Big|_{M_{\mathrm{af}},\zeta_{\mathrm{af}}} \ , \tag{5.7}$$

$Q_l(\theta)$ is already defined in Section II, and

$$\hat{P} = \frac{1}{N}\sum_{n=1}^{N} s_l(n) s_l^H(n) \ , \tag{5.8}$$

where we considered *real* signals in the *conditional* signal model (see [8]). We can generalize and use different signal models (e.g., [44]), which are extensively discussed in the literature and replace their corresponding CRB in (5.6).

Given the approximations in (5.2) and (5.3), the total probability equation at hand (5.1) can be simplified to:

$$\mathrm{MSE} \approx Pr\Big[\theta_0\Big] \ \mathrm{CRB}_l + \sum_{\kappa=1}^{\kappa_{\theta_0}} Pr\Big[\theta_\kappa\Big] \ \Big[(\theta_\kappa - \theta_0)^2\Big] \ . \tag{5.9}$$

The above expression presents an error approximate for an aliased array which operates at the frequency subband l.

Let us further simply the above equation to understand the error magnitude behavior under the aliasing scenario. We note that the probability of occurrence of the true angle is the same as the aliasing lobes assuming a noise free setup. Using this observation, the MSE approximation can be written as:

$$E\Big[(\hat{\theta}-\theta_0)^2\Big] \approx \frac{1}{\kappa_{\theta_0}} \left(\mathrm{CRB}_l + \sum_{\kappa=1}^{\kappa_{\theta_0}} \Big[(\theta_\kappa-\theta_0)^2\Big]\right) \tag{5.10}$$

Obviously, the summation term in the right hand side of (5.9) can get very large in the presence of aliasing (even as κ_{θ_0} mildly increases in the denominator according to (3.14)). This is an expected observation as the processor uses just one subband for estimation. In obtaining the above approximation, we considered the noise-free (or high SNR) assumption and we ignored the effect of the sidelobes at each subband, arguing that the discretized grating lobes, which have the same amplitude as the true lobe, have substantial impact on the error magnitude than the sidelobes. In Appendix D, we derive more accurate expressions for $Pr(\theta_0)$.

Next we will try to find an error expression, similar to Equation (5.9), when the mixture of the subbands is considered. Let us create a sample probability space by *combining* the true and the spurious aliasing angles of all subbands. We then calculate the probability of each discrete outcome θ_i^l, where $i = 0, \ldots, \kappa_{\theta_0}^l$ and $l = 1, \ldots, L$. Note that at subband l, we assign θ_0^l to be the true angle of arrival which is consistently present in all subbands. Aside from this angle all other grating lobe angles are distinct, non-repetitive and have the same *relative frequency of appearance* in our sample space (i.e., assumed equiprobable) by design (see Section B).

Let $\kappa_{\theta_0}^l$ specify the number of the aliasing angles at frequency subband l, therefore the support of the probability mixture has $\kappa_{all} + L$ members, where $\kappa_{all} = \sum_{l=1}^{L} \kappa_{\theta_0}^l$.

In the proposed method, the estimates of all subbands are incoherently combined. We can approximate the mixture and calculate the required probabilities of (5.1) using the cumulative distribution function (CDF) of binomial probability, which can be expressed in terms of the *regularized incomplete beta function*, $I_\rho(a,b)$. Therefore, the probability that the maximum occurs at the true angle after combining can be expressed as:

$$Pr[\theta_0] = I_\rho\Big(a=2,\ b=\frac{L-\rho}{\rho}\Big)\ ,\ \ \rho=\frac{L}{L+\kappa_{all}}\ , \tag{5.11}$$

where ρ is the relative occurrence frequency of the true angle in the sample space and it is considered that at least $a=2$ of the total subband estimates (i.e, $L+\kappa_{all}=a+b+1$), equal the true angle and thus form a maximum at θ_0 in the mixture. Hence, the resulting MSE approximate becomes:

$$\text{MSE} \approx Pr[\theta_0]\ \text{CRB}_e + (1\text{-}Pr[\theta_0]) \sum_{l=1}^{L}\sum_{\kappa=1}^{\kappa_{\theta_0}} \Big[(\theta_\kappa^l-\theta_0)^2\Big]\ , \tag{5.12}$$

where in the above expression, CRB_e is the equivalent alias-free CRB, which has the same half power bandwidth as the data mixture in the vicinity of the true angle (similar to (5.6)), and

$$\hat{P}_e = \frac{1}{LN}\sum_{l=1}^{L}\sum_{n=1}^{N} s_l(n)s_l^H(n)\ . \tag{5.13}$$

To understand the behavior of the processor in the asymptotic case when the number of subbands, L, gets large, we can roughly approximate the distribution of the grating lobes as discrete uniform within the scanning range, and further simplify (5.2) as:

$$Pr\Big[\theta_f\Big]\ E\Big[(\hat{\theta}-\theta_0)^2|\theta_f\Big] \approx \frac{\pi^2}{12}\sum_{\kappa=1}^{\kappa_{\theta_0}} Pr\Big[\theta_\kappa\Big]\ , \tag{5.14}$$

and hence (5.12) becomes

$$\text{MSE} \approx Pr[\theta_0]\ \text{CRB}_e + (1\text{-}Pr[\theta_0])\frac{\pi^2}{12}\ . \tag{5.15}$$

By investigating (5.15), we also observe that the aliasing angles are regarded as a nuisance to the system, since the second term dominates the MSE as SNR increases (and consequently CRB decreases). Higher SNR values will increase the magnitude of these spurious components at any given L, nonetheless regardless of the SNR, the strength ratio of these components to that of the true angle after *combining* over subbands would remain constant and would ultimately mask the noise.

Figure 10 illustrates the asymptotic behavior of the MSE estimate when L gets large using (5.12). It is seen that the overall error decreases as L increases. On the other hand, given a fixed number of the subbands, L, as SNR increases, the exceeding contributions of the aliasing noise restrict the overall performance of the processor.

This constraint does not create a burden on the application of the proposed algorithms in UWB, as the spectrum is fairly available to increase the number of subbands and, more importantly, systems with high signal strength are not applicable as secondary systems (note the power constraint in ISM [1]).

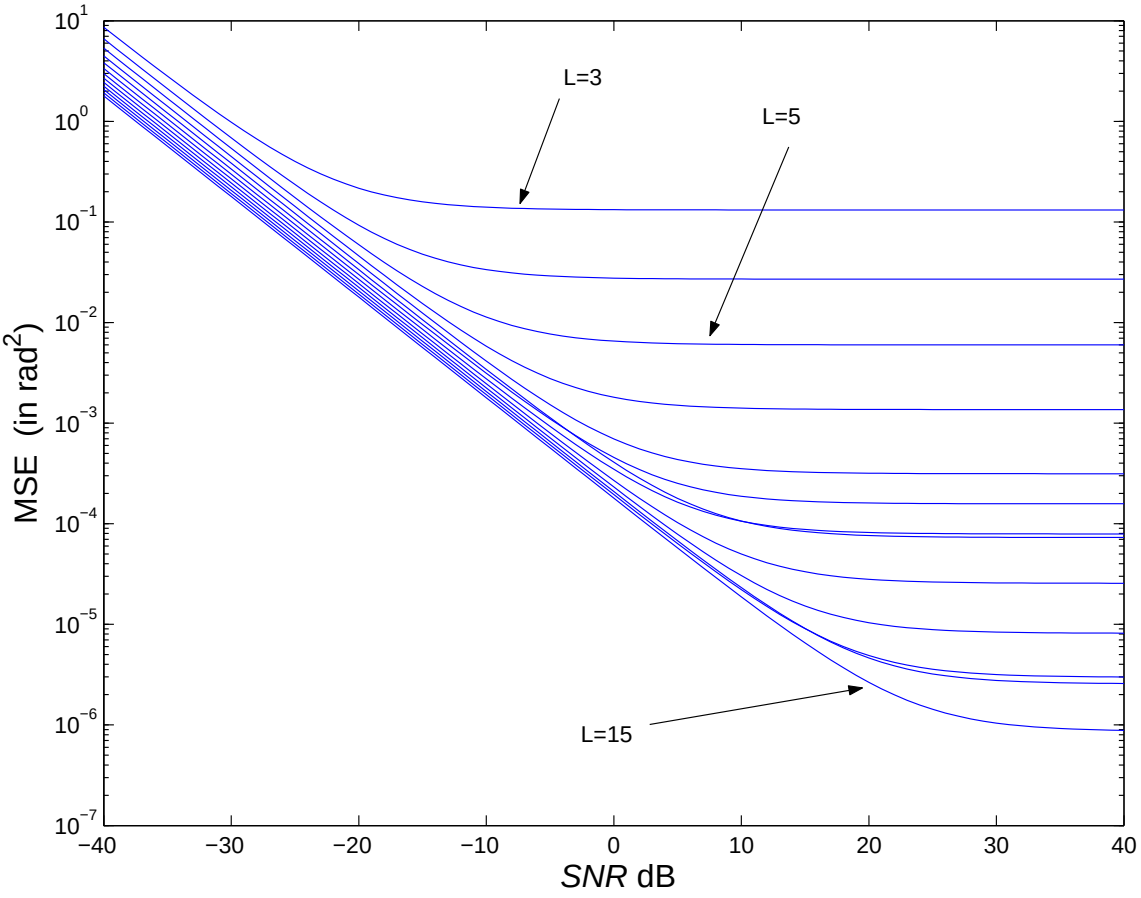

Fig. 10. The asymptotic behavior of the MSE approximation when L increases.

CHAPTER VI

SIMULATION SETUP AND RESULTS

The approaches proposed have been subjected to computer simulation experiments to study the validity of the method and the dependency of the SNR variation on the accuracy of signal and DOA estimates in terms of a simple multiple access scenario. Standard statistical measures have been used for the MLE and subspace-based algorithms.

A. MLE-based Simulation

To facilitate the demonstration we used $K = 5$ different sources, 5 different subband sets, each of them containing 20 frequency subbands ($L = 20$). The frequency subbands of the sets are spread throughout the spectrum in the following collating format: $\omega_{1,1}\ \omega_{1,2}\ \ \ldots\ \ \omega_{2,2}\ \ \ldots\ \ \omega_{4,20}\ \ \omega_{5,20}$, where $\omega_{k,l}$ is the l^{th} frequency subband from the k^{th} subband set. A ULA of $M = 10$ sensors with element spacing equal to the wavelength corresponding to the *lowest frequency* is considered. In this example, we set the lowest frequency of transmission to $\omega_{1,1} = 2\omega_{std}$, i.e., regardless of the source angle, aliasing lobes are present in all estimates. The angular granularity is set to one degree. Let us assume that the adjacent frequency difference in the above setup is fixed and equals to $\delta = 1/T_h = 0.02\ \omega_{std}$. The uncorrelated BPSK transmit sources in the experiment are assumed to have the same power with SNR= 3 dB per each subband, resting at $-50°$, $20°$, $23°$, $25°$ and $75°$ respectively relative to the broadside of the array. We use these angles to gauge the array estimates in several directions in particular in the *problematic* endfire region. It is worth reminding that the resolution of an ordinary ULA is proportional to $M\zeta_l$ in broadside region and is worse in endfire region ($\propto \sqrt{M\zeta_l}$). The interested reader may refer to Hansen-Woodyard

procedure [9], which addresses this impact in endfire arrays. Four snapshots ($N = 4$) are taken at each subband frequency for estimation of the signals and the direction of the source. Figure 11 shows the MLE-based results at each subband and the ability of the array processor to identify the direction of the transmit sources.

B. Wideband Subspace-based Simulation

For the subspace-based algorithm, a multiple source setup is considered with four wideband transmit sources ($K = 4$) or four disjoint frequency sets in observation of (3.14) and (3.15). Each of the frequency sets contains 9 frequency bins ($L = 9$). Similar to the previous setup, the frequency bins of each set are spread throughout the spectrum in a collating format. A ULA of $M = 7$ sensors is considered. The maximum adjacent frequency difference, δ, in the example setup equals to $\delta = \Delta_{max}\omega = 0.07c/d = 0.14\omega_{std}$. The angular calculation granularity is set to one degree. The uncorrelated BPSK transmit sources in the experiment are assumed to have the same power with SNR= 3 dB per each frequency bin resting at $-50°$, $20°$, $22°$ and $24°$ relative to the broadside of the array. Six snapshots ($N = 6$) are taken at each frequency bin for estimation of the signals and the direction of the source. Figure 12 shows the subspace estimation results and the ability of the array processor to identify the direction of four transmit sources.

C. Comparisons with the MSE Approximate

In order to investigate the statistical validity of these algorithms, ten thousand Monte Carlo replications are generated to measure the Mean Square Error (MSE) of both the estimated signals and the DOA with different SNRs, when one of the transmit sources is at $\theta = 22°$ relative to the broadside of an array with $M = 10$ elements,

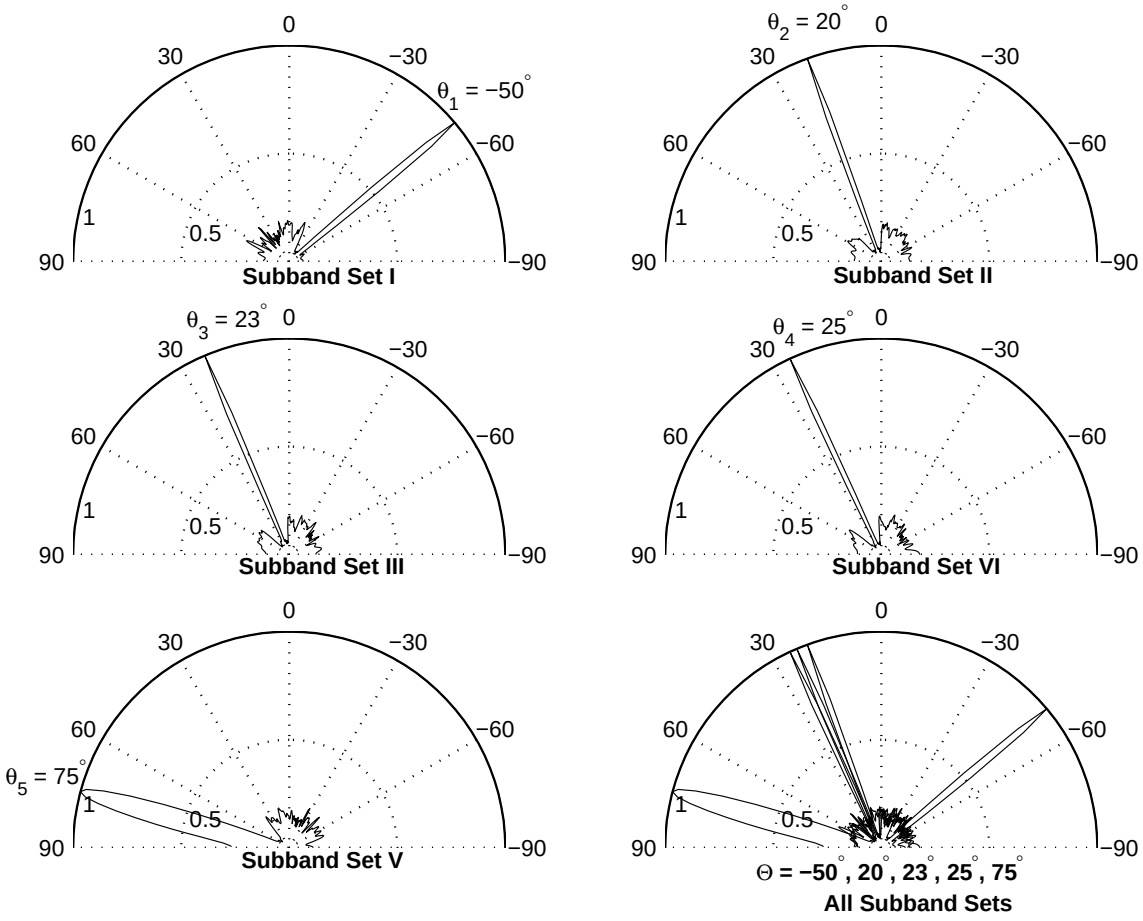

Fig. 11. The DOA estimates of 5 sources, $-50°$, $20°$, $23°$, $25°$ and $75°$ using subband hopping in 5 disjoint sets. The last figure combined the plots over each other for a better visual comparison.

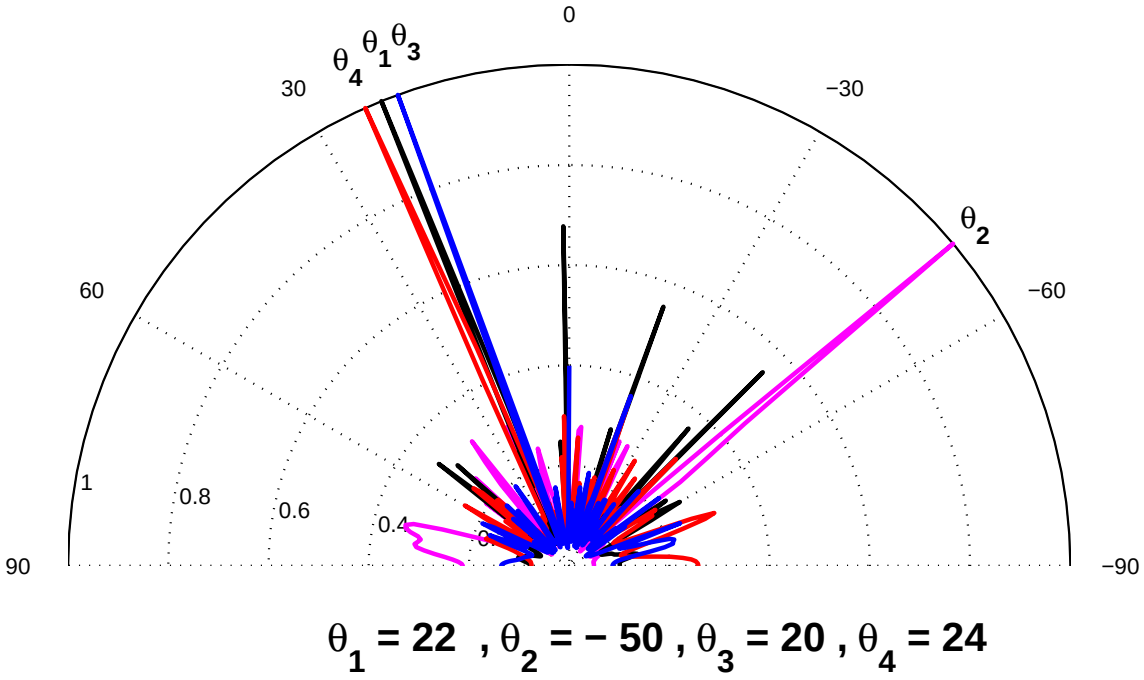

Fig. 12. An example of combined DOA estimates of 4 sources, $-50°$, $20°$, $22°$, and $24°$ using the proposed subspace method when $SNR = 3dB$, $M = 7$ (array elements), $L = 9$ frequency bins at each set and $N = 6$ snapshots at each frequency bin.

$N = 5$ and $L = 9$. The source signal uses BPSK for data transmission with a rate equal to $0.05\omega_{std}$. Figure 13 indicates the Euclidean and the Hamming distances of

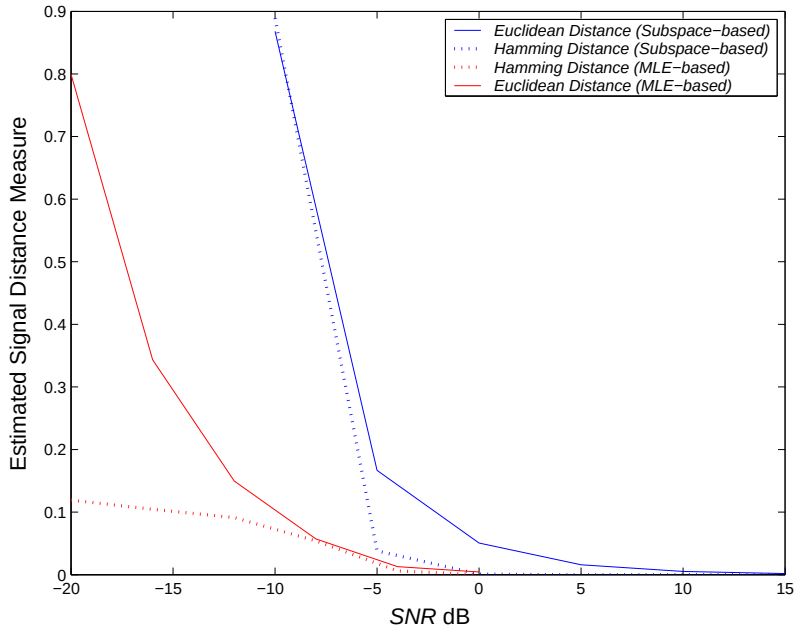

Fig. 13. Distance measures between the estimated signals and the transmitted signal versus SNR after 10000 Monte Carlo replications, for the proposed MLE-based and subband-based methods with $M = 10$, $L = 9$, $N = 5$.

the recovered signal (after BPSK demodulator) relative to the originally transmitted signal versus SNR. These distance measures are used to visually investigate the convergence and compare the performances of different estimators under the *conditional signal model*, which is assumed in this work (see e.g., [45] which assumes similar comparison metrics).

Figure 14 compares the performance of the aliased array setup when different subbands are used for transmission. We note that the processor exhibits a threshold effect at low SNR. This is a known phenomenon in the estimation theory and has been extensively discussed in the literature (see e.g., [46, 47, 43]).

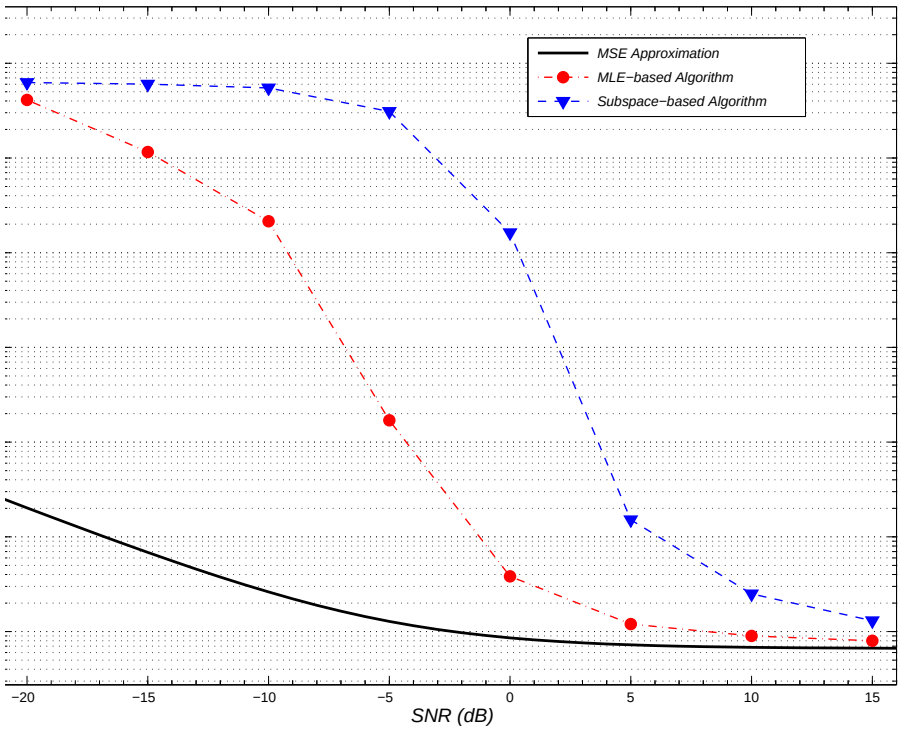

Fig. 14. MSE versus SNR for a transmitter located at 22 degrees relative to an array of $M = 10$ element, when it transmits through $L = 9$ subbands, using the MSE approximation and the simulation with 10000 Monte carlo replication. The number of snapshots is $N = 5$.

As it is seen from Figure 14, the proposed algorithms appear statistically stable, relaxing the stringent element spacing constraint, even when the number of snapshots N is relatively low. Increasing the number of snapshots, N, and the number of subbands, L, as illustrated in Figure 10 can further decrease the error magnitude.

CHAPTER VII

CONCLUSIONS AND FUTURE WORK

A. Conclusions

In this dissertation we have addressed the motives behind the use of antenna arrays in wireless networks. Based on the results of several field measurements and empirical data, we have explained that the wireless channels are becoming more and more interference–limited due to technological advances and favorable regulations. Referring to previously published results, we have further elaborated upon the fact that wideband antenna arrays could play an important (and even remedial) role in interference–limited channels, as it would enable wireless devices to utilize the inherent transmission directivity and hence operate under lower SNRs (and consequently use less power and provide better network security).

In this perspective, wideband antenna array designs and processing, which operate over a wide spectrum, have become the main focus of several academic research projects.

In another vein, element coupling among array sensors, creates – an often neglected – implementation issue in wide spectrum array structures. This is mainly due to the constraint on the element spacing, since as the frequency of transmission increases, the spacing should decrease. We discussed that the *spatial aliasing* occurs if one decides to increase the element spacing to harness the coupling impact.

This dissertation has also studied this effect of undersampling and proposed some methodologies to resolve the aliasing and ambiguity effects.

An MLE-based and a (suboptimal) subspace-based array processor have been introduced which perform DOA estimation under the aliasing scenario. A subband

hopping model for broadband sources is proposed, which is used to tackle the source association problem. This model also provides us with a more independent performance analysis of aliased arrays. The problem so formulated is shown to admit increased element spacing in uniform linear arrays (ULAs) in addition to the ability to work under low SNR. Data transmission in the proposed schemes is achieved by *multiple narrowband* frequency transmissions.

Several approximations have been considered to find an expression for the error magnitude under the aliasing scenario. The error approximate is, however, not strictly a bound but provides a relatively good benchmark and characterization of the proposed setup. The asymptotic behavior of the estimator and its relation to alias-free setup have also been also discussed.

Finally, the performances of the estimators are gauged with Monte-Carlo analysis to ensure the validity of the adopted models. The estimators inherently enjoy the source association capability and due to their hopping nature are less affected under near-far or multipath scenarios.

We also discussed how one can improve the performance of the proposed processor by an appropriate choice of the subband sets.

Although some results were obtained, there are many interesting and important problems which are left for further research, such as the possibility of coherent combining of the subbands rather than the incoherent combining under spatial aliasing.

B. Future Work

1. Constant Beam Pattern and Beam Sampling

The beam width narrows as the frequency increases from one subband to another (Figure 15). This results in different "weightings" for different subbands in combining,

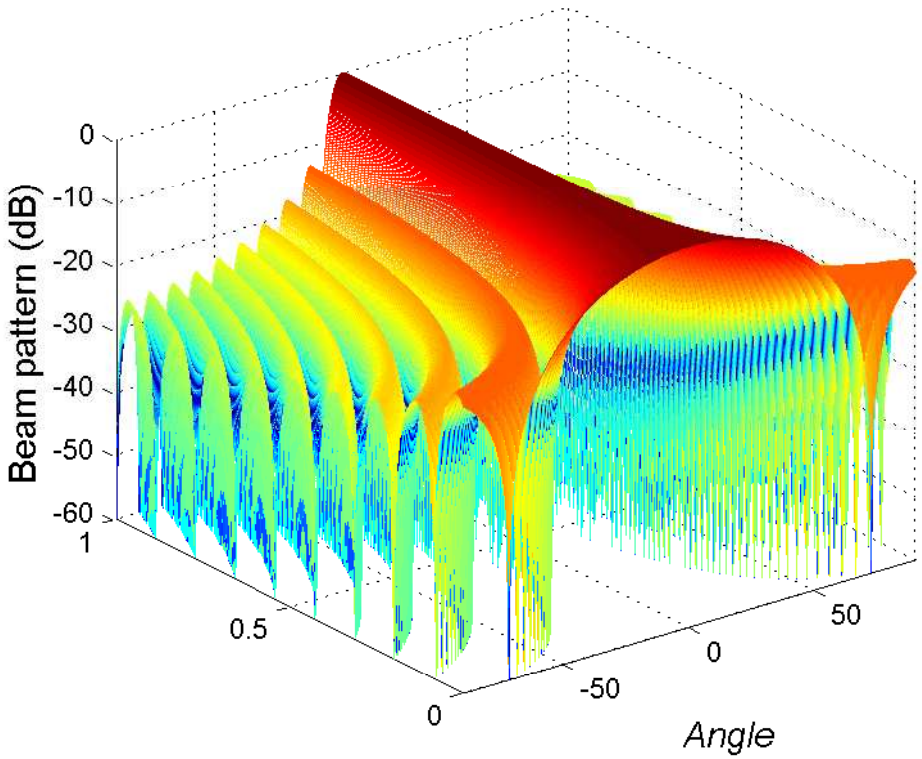

Fig. 15. Beam pattern variation as a function of frequency for an array with $M = 21$ elements (alias-free scenario).

a problem which is discussed in Section C. If we want a constant beam pattern over the frequency range, we can use beam pattern sampling techniques [22], beam-shaping filters [48], etc., to create a frequency-invariant beamformer (FIB).

Figure 16 shows an *aliased setup* after the FIB processing using [48], when the upper frequency of transmission is four times the *standard frequency* of the array. †

It appears that the beam patterns can also be sampled, under specific conditions, beyond the spatial limit. A more detailed analysis of this topic may result in better broadband arrays which can filter out the grating lobes iteratively as the array

†For derivation details, please consult with "Wideband Array processing with constant beam pattern beyond the spatial sampling" [49].

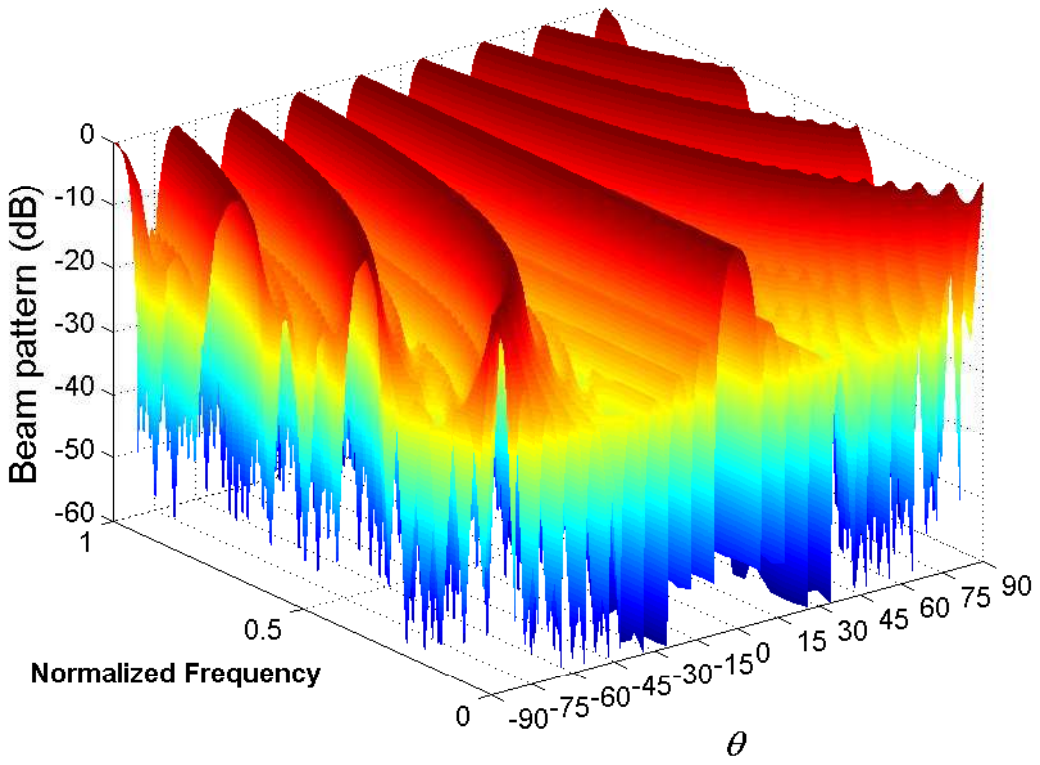

Fig. 16. Constant beam pattern after beam pattern sampling for an array with $M = 21$ elements and $L = 30$ (aliased scenario when the maximum frequency of transmission is four times the standard frequency of the array).

processor gradually receives more samples (from different subbands) in the course of time.

2. Closeness of the Grating/side Lobes

In practical implementations, although the conditions expressed in Equations (3.14) and (3.15) ensure that the grating lobe angles do not construct a maximum, due to computational constraints and given the lobe widths, some local maxima may be created, in particular when the number of the subbands is not high. The best practice in this scenario is to make sure that the generated grating lobes are maximally

distanced from each other. In this perspective, it would be helpful to develop another metric, which measures the closeness of the spurious lobes. Unfortunately due to the complex and non-linear loci of the grating lobes, a closed–form equation to describe this measure appears to be a very formidable task if not impossible. Nonetheless acquiring such measures quantitatively or qualitatively would help improving the performance of the array processor.

REFERENCES

[1] Federal Communications Commission, *Revision of Part 15 of the FCC rules regarding ultra–wideband transmission systems*, ET Docket No. 98-153, (http://www.fcc.gov).

[2] M. Kezunovic, C. Georghiades, and A. Shapoury, "Wireless communications in substations; power system monitoring using wireless substation and system-wide communications," Technical Report publication 02-46, Power Systems Engineering Research Center (PSERC), Mar. 2002.

[3] A. Shapoury and M. Kezunovic, "Field survey of wireless ISM-band channel properties for substation applications," *IEEE Power Engineering Society General Meeting*, vol. 2, pp. 1069–1074, Toronto, ON, Canada, Jul. 2003.

[4] A. Shapoury and M. Kezunovic, "Noise profile of wireless channels in high voltage substations," *IEEE Power Engineering Society General Meeting*, Tampa, FL, Jun. 2007.

[5] A. Shapoury and C. Georghiades, "A selective survey on ISM–band noise profile measurement and forecasting," *SPIE International Symposium, Noise in Communication Systems*, Austin TX, May 2005.

[6] P. Gupta and P.R. Kumar, "The capacity of wireless networks," *IEEE Transactions on Information Theory*, vol. 46, no. 2, pp. 388–404, Mar. 2000.

[7] M. Grossglauser and D. Tse, "Mobility increases the capacity of adhoc wireless networks," *IEEE/ACM Transactions on Networking*, vol. 10, no. 4, pp. 477–486, Aug. 2002.

[8] H.L. Van Trees, *Optimum Array Processing: Detection, Estimation, and Modulation Theory*, New York: John Wiley & Sons, 2002.

[9] C.A. Balanis, *Antenna Theory : Analysis and Design*, Hoboken, NJ: Wiley-Interscience, 3rd edition, 2005.

[10] I.J. Gupta and A.A. Ksienski, "Effect of mutual coupling on the performance of adaptive arrays," *IEEE Transactions on Antennas and Propagation*, vol. 31, no. 5, pp. 785–791, Sep. 1983.

[11] R. Janaswamy, "Effect of element mutual coupling on the capacity of fixed length linear arrays," *IEEE Antennas Wireless Propagation Letters*, vol. 1, no. 1, pp. 157–160, 2002.

[12] M.A. Jensen and J.W. Wallace, "A review of antennas and propagation for MIMO wireless communications," *IEEE Transactions on Antennas and Propagation*, vol. 52, pp. 2810–2824, Nov. 2004.

[13] T. Svantesson and A. Ranheim, "Mutual coupling effects on the capacity of multielement antenna systems," *2001 IEEE International Conference on Acoustics, Speech, and Signal Processing (ICASSP '01)*, vol. 4, pp. 2485–2488, Salt Lake City, UT, May 2001.

[14] M. Agrawal and S. Prasad, "Broadband DOA estimation using spatial–only modeling of array data," *IEEE Transactions on Signal Processing*, vol. 48, no. 3, pp. 663–670, Mar. 2000.

[15] H. Wang and M. Kaveh, "Coherent signal subspace processing for detection and estimation of angle of arrival of multiple wideband sources," *IEEE Transactions on Acoustics, Speech, Signal Processing*, vol. ASSP–33, pp. 823–831, Aug. 1985.

[16] L. Xiangqian, N.D. Sidiropoulos, and A. Swami, "Blind high-resolution localization and tracking of multiple frequency hopped signals," *IEEE Transactions on Signal Processing*, vol. 50, no. 4, pp. 889–901, Apr. 2002.

[17] A.N. Amini and T.T. Georgiou, "Avoiding ambiguity in beamspace processing," *IEEE Signal Processing Letters*, vol. 12, no. 5, pp. 372–375, May 2005.

[18] R.O. Schmidt, "Multiple emmiter location and signal parameter estimation," *IEEE Transactions on Antennas and Propagation*, vol. AP–34, no. 3, pp. 276–280, Mar. 1986.

[19] K.T. Wong and M.D. Zoltowski, "Extended-aperture underwater acoustic multisource azimuth/elevation direction–finding using uniformly but sparsely spaced vector hydrophones," *IEEE Journal of Oceanic Engineering*, vol. 22, no. 4, pp. 659–672, Oct. 1997.

[20] K.-C. Tan, G.-L. Oh, and M. H. Er, "A study of the uniqueness of steering vectors in array processing," *Signal Processing*, vol. 34, no. 3, pp. 245–256, Dec. 1993.

[21] T. Chou, "Frequency-independent beamformer with low response error," *IEEE International Conference on Acoustics, Speech, and Signal Processing*, vol. 5, no. ICASSP-95, pp. 2995–2998, Detroit, MI, May 1995.

[22] M.M. Goodwin and G.W. Elko, "Constant beamwidth beamforming," *IEEE International Conference on Acoustics, Speech, and Signal Processing*, vol. ICASSP–93, pp. 169–172, Minneapolis, MN, Apr. 1993.

[23] R.S. Tahim, J. Foshee, and K. Chang, "Networking of multi-band phased array antennas for mobile communication," *IEEE International Symposium on*

Antennas and Propagation Society, vol. 2, pp. 468–471, Columbus, OH, Jun. 2003.

[24] J. Foshee, R.S. Tahim, and K. Chang, "Networking highly mobile users using several multi-band phased array antennas," *Proceedings of the 44th IEEE 2001 Midwest Symposium on Circuits and Systems*, vol. 1, pp. 409–412, Dayton, OH, Aug. 2001.

[25] M. Wax, T.J. Shan, and T. Kailath, "Spatio–temporal spectral analysis by eigenstructure methods," *IEEE Transactions on Acoustics, Speech, Signal Processing*, vol. ASSP–32, pp. 817–827, Aug. 1984.

[26] P.J. Chung, J. F. Boehme, and A. O. Hero, "Localization of multiple moving sources using recursive EM algorithm," *EURASIP Journal on Applied Signal Processing*, vol. 1, pp. 50–60, Jan. 2005.

[27] R. Roy and T. Kailath, "Espritestimation of signal parameters via rotational invariance techniques," *IEEE Transaction on Acoustics, Speech, Signal Processing*, vol. 37, pp. 984–995, Jul. 1989.

[28] K.M. Buckley and L.J. Griffiths, "Broad-band signal-subspace spatial-spectrum (BASS–ALE) estimation," *IEEE Transactions on Acoustics, Speech, and Signal Processing*, vol. 36, no. 7, pp. 953–964, Jul. 1988.

[29] M. Kaveh and A. J. Barabell, "The statistical performance of the MUSIC and the minimum–norm algorithms in resolving plane waves in noise," *IEEE Transactions on Acoustics, Speech and Signal Processing*, vol. 34, no. 2, pp. 331–341, Apr. 1986.

[30] K.M. Buckley, "Spatial/spectral filtering with linearly constrained minimum

variance beamformers," *IEEE Transactions on Acoustics, Speech, and Signal Processing*, vol. 35, no. 3, pp. 249–266, Mar. 1987.

[31] P. Stoica and R. Moses, *Spectral analysis of signals*, Upper Saddle River, NJ: Prentice Hall, 2005.

[32] R. Voges and J. Butler, "Phase optimization of antenna array gain with constrained amplitude excitation," *IEEE Transactions on Antennas and Propagation*, vol. 20, no. 4, pp. 432–436, Jul. 1972.

[33] K. Keen, "On the equivalent aperture formation of an endfire array," *IEEE Transactions on Antennas and Propagation*, vol. 22, no. 6, pp. 831–832, Nov. 1974.

[34] A. Shapoury and E. Serpedin, "Incoherent DOA estimation in uniform antenna arrays with inordinate spacing using a subband hopping approach," *Journal of Circuits, Systems, and Signal Processing*, 2007, (Submitted).

[35] A. Shapoury, "Incoherent MLE of array antennas with inordinate spacing using subband hopping approach," in *64th IEEE Vehicular Technology Conference*, Montréal, QC, Canada, Sep. 2006.

[36] P. Stoica and A. Nehorai, "Music, maximum likelihood, and Cramèr–Rao bound," *IEEE Transactions on Acoustics, Speech, and Signal Processing*, vol. 37, no. 5, pp. 720–741, May 1989.

[37] A. Manikas and C. Proukakis, "Modeling and estimation of ambiguities in linear arrays," *IEEE Transactions on Signal Processing*, vol. 46, no. 8, pp. 2166–2179, Aug. 1998.

[38] K.-C. Tan, S.S. Goh, and E.-C. Tan, "A study of the rank–ambiguity issues in direction–of–arrival estimation," *IEEE Transactions on Signal Processing*, vol. 44, no. 4, pp. 880–887, Apr. 1996.

[39] R.O. Duda, P.E. Hart, and D.G. Stork, *Pattern Classification*, New York: John Wiley & Sons, 2nd edition, 2000.

[40] M. Viberg, B. Ottersten, and A. Nehorai, "Performance analysis of direction finding with large arrays and finite data," *IEEE Transactions on Acoustics, Speech, and Signal Processing*, vol. 43, no. 2, pp. 469–477, Feb. 1995.

[41] A. Shapoury, "A subspace approach for DOA estimation of uniform linear arrays with increased element spacing applicable to wideband transmission," *IEEE/CreateNet International Conference on Broadband Networks*, vol. 2, pp. 1188–1193, Boston, MA, Oct. 2005.

[42] L. Hong and K.C. Ho, "Classification of BPSK and QPSK signals using an antenna array," *Journal of Circuits, Systems, and Signal Processing*, vol. 24, no. 4, pp. 343–361, 2005.

[43] D.C. Rife and R.B. Boorstyn, "Single–tone parameter estimation from discrete–time observations," *IEEE Transactions on Information Theory*, vol. 20, no. 5, pp. 591–598, Sep. 1974.

[44] S.F. Yau and Y. Bresler, "A compact Cramèr–Rao bound expression for parametric estimation of superimposed signals," *IEEE Transactions on Acoustics, Speech, Signal Processing*, vol. 40, pp. 1226–1229, May 1992.

[45] J. Li and D. Zheng, "Parameter estimation using RELAX with a COLD array," *Journal of Circuits, Systems, and Signal Processing*, vol. 17, no. 4, pp. 27–45,

Jul. 1998.

[46] F. Athley, "Threshold region performance of maximum likelihood direction of arrival estimators," *IEEE Transactions on Signal Processing*, vol. 53, no. 4, pp. 1359–1373, Apr. 2005.

[47] L. Knockaert, "The Barankin bound and threshold behavior in frequency estimation," *IEEE Transactions on Signal Processing*, vol. 45, no. 9, pp. 2398–2401, Sep. 1997.

[48] D.B. Ward, Z. Ding, and R.A. Kennedy, "Broadband DOA estimation using frequency invariant beamforming," *IEEE Transactions on Acoustics, Speech, and Signal Processing*, vol. 46, no. 5, pp. 1463–1469, May 1998.

[49] A. Shapoury and E. Serpedin, "Wideband array processing with constant beam pattern beyond the spatial sampling," *IEEE International Conference on Signal Processing and Communications*, vol. ICSPC 2007, Dubai, UAE, May 2007, (Submitted).

[50] N.G. Riley and K. Docherty, "Modeling and measurement of man-made radio noise in the VHF-UHF band," in *Ninth International Conference on Antennas and Propagation*, Eindhoven, The Netherlands, Apr. 1995.

[51] E.N. Skomal and A. Smith Jr., *Measuring the Radio Frequency Environment*, New York: Van Nostrand Reinhold Company, 1985.

[52] R.J. Achatz, Y. Lo, P.B. Papazian, R.A. Dalke, and G.A. Hufford, "Man-made noise in the 136 to 138-MHz VHF meteorological satellite band," Research Report 98-355, The National Telecommunications and Information Administration (NTIA), Oct. 1998.

[53] E.N. Skomal, *Man-Made Radio Noise*, New York: Van Nostrand Reinhold Company, ISBN 0-442-27648-6 edition, 1978.

[54] M. Nordman, T. Nieminen, and M. Lehtonen, "Characteristics of wireless sensors in electrical distribution networks," *IEEE Conference on Mechatronics and Robotics*, pp. 1–7, Aachen, Germany, Sep. 2004.

[55] M.K. Simon, J.K. Omura, R.A. Scholtz, and B.K. Levitt, *Spread Spectrum Communications Handbook*, New York, NY: McGraw–Hill, 2002.

[56] Institute of Electrical and Electronics Engineers (IEEE), *Recommended practice for an electromagnetic site survey (10 kHz to 10 GHz)*, IEEE Std 473-1985, Jun. 1985.

[57] Federal Communications Commission (FCC), *47 CFR, PART 15 Radio Frequency Devices*, Revised October 1, 2006.

[58] K.S. Gilhousen, I.M. Jacobs, R. Padovani, A.J. Viterbi, L.A. Weaver, and C.E. Wheatley III, "On the capacity of a cellular CDMA system," *IEEE Transactions on Vehicular Technology*, vol. 40, no. 2, pp. 303–312, May 1991.

[59] G. E. P. Box, G. M. Jenkins, and G.C. Reinsel, *Time Series Analysis, Forecasting and Control*, Englewood Clifs, NJ: Prentice Hall, 3rd edition, 1994.

[60] Institute of Electrical and Electronics Engineers (IEEE), *Standard procedures for the measurement of radio noise from overhead power lines and substations*, ANSI/IEEE STD 430-1986, Feb. 1986.

[61] Institute of Electrical and Electronics Engineers (IEEE), *Standard definitions of terms relating to Corona and field effects of overhead power lines*, Revision of ANSI/IEEE Std 539, 1990.

[62] C.M. Bishop, *Neural Networks for Pattern Recognition*, New York: Oxford University Press, 1995.

[63] R.E. Shaffer, S.L. Rose-Pehrsson, and A. McGill, "A comparison study of chemical sensor array pattern recognition algorithms," *Analytica Chimica Acta*, vol. 384, no. 3, pp. 305–317, Apr. 1999.

[64] J. Proakis, *Digital Communications*, New York, NY: McGraw–Hill, 4th edition, 2000.

APPENDIX A

FIELD SURVEY OF WIRELESS ISM-BAND CHANNEL PROPERTIES*

PREFACE

In an interdisciplinary project to gauge the wireless channel quality in electric power substations, several setup configurations were designed to collect the empirical characteristics of wireless channels in several locations. This section discusses the motive, setup and the result of this investigation. Leaving aside the importance of such field measurements for specific applications, the findings suggest that the *unwanted signals* (i.e., interferences plus noise), have strong time-dependant characteristics. Environmental data has been collected to investigate any correlation between the unwanted signal levels (i.e., noise plus interference) and the variance variations of the Gaussian random noise (i.e.,"noise only" variation due to environmental or atmospheric changes). The results suggest that the unwanted power level exhibits little correlation with the random noise and more with the setup location, i.e., industrial, residential and sparsely populated regions. This strongly implies that the dominant constituents of the unwanted signals are interference–related rather than noise–related.

* This work was sponsored by Power Systems Engineering Research Center (PSERC), National Science Foundation Industry/University Collaborative Research Center under grant NSF EEC-0002917. The Office of the State Climatologist (OSC) for Texas provided us with the surface weather data.

Abstract *

In this survey, some measuring metrics are identified to study the average noise power variations in typical outdoor power substations. Power substations generally have metallic structures and despite the insulation considerations have high electric fields. The physical size of a substation does not allow a completely controlled experiment. A setup plan was arranged to study the noise floor variation in a few substation switchyards in residential, industrial, isolated and sparsely populated subdivisions. The empirical data sets were collected, processed and compared with the known noise constituents that were cited in the literature. A two-week measuring window was chosen to encounter any possible factors that might affect results at several substations. Several field measurements were executed to enable the comparative analysis of the recorded data. By collecting the weather data during the survey, it was illustrated that the average noise floor in the spectrum of interest (i.e., 2.4 GHz), does not correlate or has week correlations with the real time weather condition changes, such as humidity, pressure and precipitations. The analysis suggests that the noise floor variation (and hence the link quality) is time-dependent and has an underlying dominant semi-deterministic constituent in addition to the classical random distribution. This semi-deterministic component is associated with the location of the substation switchyard (e.g., residential or industrial), and its dynamic range is significant and should be identified. The methodology, which is adopted in this study has applications in the analysis of static outdoor environments. Several practical considerations have been discussed in this work for future implementations in high electromagnetic

*©2007 IEEE. Reprinted, with permission, from "Noise Profile of Wireless Channels in High Voltage Substations", Alireza Shapoury and Mladen Kezunovic, IEEE Power Engineering Society General Meeting (PESGM'07), June 2007 (accepted for publication at the time of this dissertation).

field environments.

Introduction

Wireless networks have several features that make them an attractive communication solution in the harsh industrial environment such as electrical distribution or transmission networks. Since wireless networks do not use expensive signal and control cables for data transmission, they are easier to install and use, and hence provide a cost effective solution for industrial and power system applications. The utilization of the existing wireless technologies should be closely investigated to better understand the detrimental impacts of switching transient fields on the radio band channels [50, 51, 52, 53, 54]. An accurate analysis for comparing different wireless implementations requires measurement and inspection of a wide spectrum of modulation, coding and implementation techniques. Metallic structure, electric impulses from the corona effect or switching operations of power apparatus, and electromagnetic interferences and weather variations are among the discriminative features in this particular industrial environment. From theoretical standpoint, the wireless receivers are often designed based upon certain assumptions about noise [55]. Most of them assume that noise is IID (Independent Identically Distributed) and has some form of exponential-family distribution such as Guassian or Rayleigh. Some others consider correlated noise but with specific autocorrelation properties. Some noise distributions contribute to the noise floor. Other noise profiles may produce impulsive disruptions of links, for instance the Poisson-Gauss model [52].

The validity of the scientific conclusions becomes intrinsically linked to the validity of these underlying assumptions. In practice, since some of the assumptions are unknown or untested for specific applications, the scientific conclusions become arbitrary. A good estimate of the noise pattern is the target of this study. If there

is a good estimate of the noise pattern, then we can calculate the error rate under a given channel-coding scheme. We prefer not to do the reverse, i.e., estimate the noise profile by just observing the resulting calculated and processed error rates, in particular when an estimate of the noise profile is directly obtainable.

To assess the characteristics of the wireless network, field experiments were conducted with spread spectrum radios operating at 2.4 GHz. A special attention was paid to long term observations. For instance, long period measurement runs allows us to observe the variation of average noise power during the weekdays. In some applications, the impact on wireless devices needs to be attributed to portable structures as opposed to constantly moving (or mobile) objects (e.g., cellular phones). In this approach, measurements were made for a period of fourteen days, with both moving transceivers (on a wheel-cart to facilitate repositioning) and fixed location transceivers in critical locations, for example, in the vicinity of a circuit breaker.

There are some recommendation practices in the literature for the site surveys, which are primarily based on the Bayesian probability assumptions of the noise. In the observation of such recommendations (e.g., in [56], field surveys, tests and cross-validations were performed and reported in [3]. It is shown that despite the soundness of the recommended *Kolmogorov-Smirnov Test (KS test)* based on the Bayesian assumption, the average noise power variation at 900MHz Industrial, Scientific and Medical frequency bands (ISM [57]) has typically stronger time-series constituent and can therefore be approximated by an Auto-Regressive Moving Average (ARMA) model. This finding has some implications in the design of wireless systems. For instance in CDMA applications [58], to avoid the capacity degradation, power control schemes are used to improve power efficiency and the connectivity by addressing the near-far problem. The semi-deterministic nature of the noise floor which is further addressed in the present study, relates to the dynamic range of the power control

schemes.

Admittedly, due to the large physical size of the test environment, the measurement was not a controlled test process (i.e., *controlled experiment* [59]) in which one could acquire and record all the relevant environmental and electrical parameters (e.g., delay profile). In this study, as much information about the test and as much analysis as possible is gathered to supplement anecdotal evidence used in the past.

In the first part, the probable impacts of the industrial environment on the wireless channel are investigated considering the observation windows based on previously published measurements, analyses and pertinent assumptions found in the standards and technical literature [53, 55, 60, 61]. The data recording plan and disposition of test devices is discussed next. Description of how the data was *conditioned* and preprocessed to enable an accurate analysis is given in a follow up section. Subsequently, statistical data analysis and comparison of the performance of different analyses approaches are presented. The simulation results and the conclusion are given at the end.

Noise Pattern Constituents

One particularly detrimental characteristic of the (wireless) channel of interest is the presence of ambient electromagnetic interference (EMI) produced by power lines and power apparatus used for switching the substation configuration. The electromagnetic fields radiated by these interfering sources may occur as spurious signals and, hence, are a source of noise [60]. In radio transmission we are especially concerned about the electromagnetic noises which are non-stationary in nature. There are two main types of radiated radio noise sources in substations: gap breakdown and line conductor corona [53].

Gap discharge radio-noise is produced by a rapid flow of electric current in the air gap between two points of unequal potential occurring on electric power switching equipment. The current-surge accompanying avalanche ion production is of very brief duration, consisting of one or several impulses persisting for a few nanoseconds. These noises are strongly impulsive in nature. The statistics of this phenomenon are directly related to the electrical incidents, and result in opening or closing of switching elements commonly called circuit breakers.

Corona discharge is also a threshold transition process that requires a critical potential gradient in the vicinity of a charged object be exceeded before the effect is manifested. The charged object needs not be an electrical conductor.

Either source may be comparable or exceed the noise power levels of other man-made noise sources. A noise source might create impulsive noise in one system and a random noise in a different system (for instance as in Frequency Hopping Spread Spectrum systems versus Direct Sequence Spread Spectrum [2]). A strong impulsive noise may create a uniform disturbance over the frequency spectrum of interest. The radio noise produced by these phenomena exhibit RF components of substantial magnitude in the UHF-TV band (470-806 MHz) [52].

This study does not suggest the importance of the impact of the gap breakdown (e.g., circuit breaker operations) on the wireless channel due to the scarcity of the phenomenon, nor does it probe the absolute value of the corona discharge. In normal operations, the corona discharge is the discriminatory phenomenon between the power substations environment and other industrial environments, which are already studied in the literature. This survey was to investigate whether the variation of the corona discharge has an effective impact on the variation of the noise power. In general, we expect to observe three types of noises in substation applications: background noise, incidental impulsive noise and unwanted signals. In this study, the background

noise is defined as the total sources of disturbances in the link and the measurement system, independent of the presence of the signal. For instance the Trichel streamers and glow corona contribute to this background noise. The incidental impulsive noise is due to the gap breakdown discharge phenomena (often caused by circuit breaker opening). The ideal method of tracking these phenomena is to apply fast response measuring devices (i.e., peak detectors) for long runs and record the receptions during breaker opening, as well as investigating the seasonal effects and climate impacts. In power-line applications, random noise (often considered Gaussian) is a component of the total noise caused by the discharge [61]. Hence the average noise level indicates the level of background noise and interference at the measurement site. It is worth noting that there is little or no (slow or fast) fading due to the stationariness of the devices in substations. The testing periods were chosen to be long enough to include atmospheric cycle extremes, and probable diurnal and weekly patterns.

Test Setup Plan

The measurement setup was designed by using readily available instruments while considering the size of substation yards and the presence of high power signals. Surges initiated by the power system and ground leakage currents can damage the measuring devices, therefore appropriate grounding and protection have been incorporated in the setup design (Figure 17).

The main methods of high voltage surge protection are the *series* and the *shunt* approaches. Series devices are typically designed or plugged directly into the Radio Frequency (RF) line between the antenna and the RF circuitry attempting to block the incoming surges before they reach the RF amplifier. In the shunt approach, the surge is guided away from the RF input by providing a better path to ground.

The use of Quarter-wave stubs is a popular method among the RF design engi-

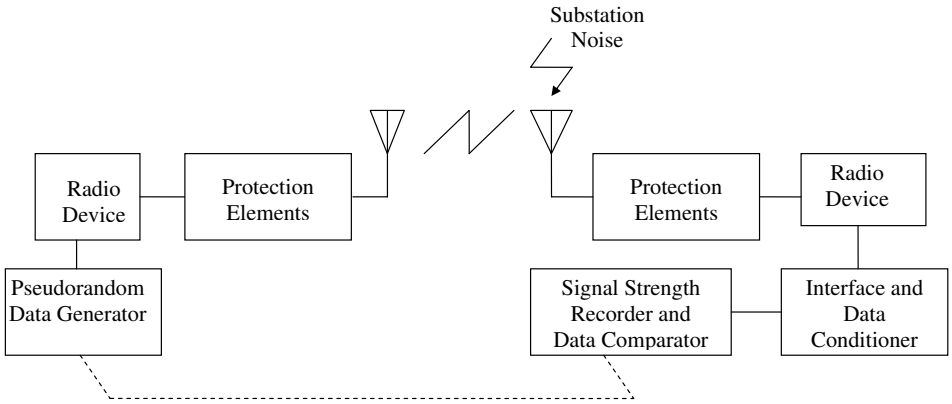

Fig. 17. Measurement block diagram.

neers which could be realized in series or shunt configurations. A quarter wave stub protector creates a band-pass filter focused at the center frequency of the wireless device. Notwithstanding the low-frequency attenuation of the stubs, a detrimental portion of the energy could still enter the equipment input (Note that the voltage and energy levels are too high for sensitive RF front-end even given significant attenuation).

Gas-Tubes and Non-Gas Tubes protection devices are among other elements which limit the let-through voltage into the sensitive RF circuitry by exhibiting a Zener-like breakdown phenomenon. These devices are seldom built-in and need to be attached externally.

In this survey, a setup plan is conducted for the 2.4 GHz frequency band using IEEE802.11 compatible radios. In the preliminary test implementations, none of the aforementioned methods exclusively secured the setup against the detrimental surges in the substations, ultimately causing some equipment damage and failures. Our conjecture is that the impulsive noise in the substations is too fast to be contained

with DC-blocks alone and is too strong over the time to be contained solely by the Quarter-wave stubs. Hence a combination of the protection methods is used in the final setup and is suggested for future implementations.

The linearity of these protection provisions needs to be considered to avoid skewing the recorded data within the frequency spectrum.

The setup consists of wireless modems (acting as access units and base units), data acquisition devices and a processing unit (Figure 18). The access unit was placed next to the control room (where the base unit is more likely to be located) with an omni-directional antenna attached to it. Note that the physical structure of a typical substation or an industrial environment may not allow the use of directional antennas. The subscriber unit was placed at the far end of the substation, attached to a metallic structure (i.e., the circuit breaker panel). The device disposition was such that there was no line of sight communication. The power control feature in the communication device is inhibited and the signal power is maintained constant during the trial. The processing unit fetches the wireless quality parameters from the modems. The data are then automatically recorded on a laptop machine for post-processing. Two laptops were deployed and programmed to emulate the continuous data communication to the virtual circuit breaker receiver and to handle the logging and background processing. Figure 19 shows typical dispositions of the radio transceivers. The in-yard radio was installed 1.2m above the ground level and electrically attached and grounded to the metallic structures of the circuit breaker (Since the wireless communication analysis is aimed at monitoring operation of circuit breakers, free-body metering suggested in [56] would be inappropriate in this case).

The survey duration of the measurement run was about 14 days in each yard (i.e., the 34.5 KV, 138 KV and 345 KV yards) to include weather cycle extremes, and probable diurnal and weekly patterns.

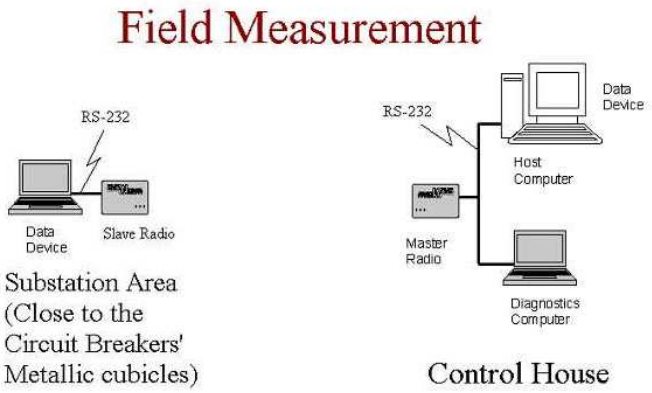

Fig. 18. 2.4 GHz measurement setup.

Data Recording and Pre-processing

The main objective of this survey is studying the variations of the noise floor levels rather than the absolute magnitudes of the measured parameter. In most wireless design quality analysis, the magnitude of the Signal to Noise ratio (S/N) and Signal to Interference ratio (S/I) are of more importance than the absolute values of signal, interference and noise levels individually.

The results presented in this paper have been generated using the observed data collectively. There was no electrical incident or breaker operation during this survey, and hence there is no major gap-breakdown noise (i.e., as mentioned before these incidents are rare in nature). Other than that, the wireless devices seemed to receive no disturbing high power noise impulses due to the high voltage (HV) corona effect, which could cause major link disruption. The higher the voltage level, the higher average noise was observed.

The polled signal levels from the radios are in Receiver Signal Strength Indicator (RSSI) format, which are often in linear or in logarithmic format. RSSI is used in the control loop of the firmware of the radio. Manufacturers do not usually calibrate

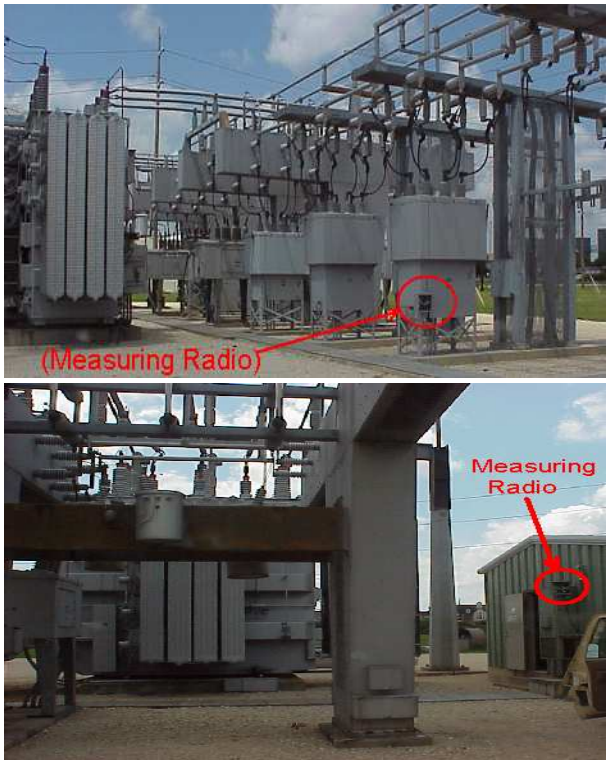

Fig. 19. No-line-of-sight (NLOS) disposition of the instruments in a power substation.

the RSSI of their radios to dBm values, and often instead provide an approximate conversion table for the mapping between these values. Since RSSI is a relative index, the device works regardless of RSSI calibration to dBm values and hence it was assumed that the measurement setup was subject to the offset (calibration) error. This error has been ignored as the general methodology adopted is invariant to this offset error and the background noise may anyway induce offset in different locations. The level calculations are implemented by utilizing the conversion table and then converting the dBm values to the desired voltage levels. The recorded data from this experiment have been utilized for the 2.4 GHz analyses. Each reading takes approximately one second which contains the exact timing information. The average noise power, in this survey, is calculated as the average noise level in the transmission

spectrum and is recorded in one-minute intervals as a moving average of 60 readings (i.e., window size). The radios use 79 channels in the 2400 to 2483.5 MHz frequency range using 9 hopping sequences per each hopping set. A program has been designed to continuously poke the link quality data from the radios, seeing that this feature was not a built-in function in the device. Specific provisions were made to avoid data congestion while polling the data from the radios. In this regard there were just two wireless devices at each measurement run in the substation yard and the baud rate of the dummy data generator is set constant and low. The processing unit also handled the data logging. As test duration was fourteen days, there were more than 20,000 observations per each data set.

It is reported that the weather conditions drastically affect the noise generation in high voltage outdoor environments [61]. To include the environmental impacts on the wireless channel, dew point, dry bulb and wet bulb temperatures, station and sea level pressures, and the relative humidity and the presence of any precipitation during the observation window have been incorporated in the analysis on an hourly basis. These surface weather data have been recorded on hourly basis through the three nearest weather stations, which have at most 12.4 miles aerial distance to the test site. Note that the rates of changes of environmental data are typically low and the variations (and not the mean) of the surface data in these closely spaced weather stations are almost similar. This data resolution is accurate enough due to the tardiness of the atmospheric changes. To relate the weather parameters to the average SNR variation, pre-processing of data was done such that the data sets have similar timings (i.e., observation windows). The resulting weather data has less timing resolution than the electrical data (e.g., the load pattern of the transformers in the substation and the recorded SNR values).

To calculate an approximate estimate for the (higher resolution) electrical data

coinciding with the weather hourly data, Parzen window [62] with smoothing parameter of $h = 60$ (minutes) has been used. We define the Parzen Kernel function $\varphi(u)$ such that:

$$\varphi(u) = \begin{cases} 1 & \mid u \mid < \frac{1}{2} \\ 0 & \text{otherwise} \end{cases} \tag{A.1}$$

then the estimated values at the hourly grid points, x_H, would be:

$$x_H = \frac{1}{Nh} \sum_{m=1}^{N} x_m \varphi(\frac{H-m}{h}) \tag{A.2}$$

where N is the total number of samples with higher resolution (i.e., observations with one-minute precision), x_m is the magnitude of the m^{th} sample, and x_H is the new generated sample with lower resolution (i.e., one-hour precision). Thus the resulting size of the data set becomes 340 samples. We can use other types of Kernels such a Gaussian [62], but we found little variations in our final result to justify the use of more complex Kernels.

Table I lists the observed parameters and the experiment settings. The dynamic range of the noise variation has particular significance, when a wireless *Power Control* scheme is considered, the dynamic range together with the wireless circuit *design constraints* prescribe the step-size and the granularity of the power control. Without loss of generality, it is assumed that the wireless devices have five *power steps* within their dynamic range and hence five classes are assigned for this survey.

Data Analysis

The goal of this study is to probe the predictability of the noise floor level (note that the power control is disabled and since the signal levels are constant during the transmission, the SNR variations are proportional to noise variations). To this end, several classifiers have been considered given the observation parameters and then

Table I. The observed parameters and the settings.

Observation parameters	Setting
SNR	Observation size= 333 samples,
Dew point temperature	Training percent =13/14 (Hold-Out Method)
Relative humidity	KNN neighbor = 1
Sea level pressure	5 noise classes
Station pressure	
Wet bulb temperature	
Dry bulb temperature	
Dew point temperature	
Presence of precipitation	
Transformer load patterns	
Time	

their classification rates have been gauged. The success of a classifier in having higher classification rate could reveal the underlying structure of the data. As mentioned before, the inertness of one observation parameter can be determined if the omission of that parameter does not substantially change the classification rate of the chosen best classifier.

The data set is divided to the training set and the test set using the *hold-out* method [39]. 90% of the data is considered for the training and the remaining for the testing purpose. Quadratic and K-Nearest Neighbor (KNN) classifiers are used as pattern classifiers [63].

Some of the observation parameters may not affect the process or have less impact as they may act similar to random noise in our process. The issues regarding

the correlation, causality, the common cause scenarios, and confounding and coincidental factors are also addressed in the analysis. Some observation parameters are inter-correlated. Given the actual station pressure and the wet bulb and the dry bulb temperatures, the dew point and relative humidity can be calculated. We did not know this underlying relation when we gathered the weather data. This is an apparent example of correlation, which may exist in the observation. We kept all the observation parameters and could investigate if the chosen"best classifier" is robust to these discrepancies in the observation data. (One can always compare the results to the case when these correlations are known a priori).

Feature extraction

In practice, there is a maximum number of features above which the performance of any classifier will degrade rather than improve. This phenomenon is due to the fact that blindly increasing the number of features (as also exemplified above with the weather data), may allow correlated features and the noise to incorporate in the classification process. To remedy the problem, feature extraction which transforms the existing features into a lower dimensional space that preserves most of the information in the original samples x has been performed.

$$f : x \in \mathcal{R}^{\Omega} \longrightarrow y \in \mathcal{R}^{\Pi} \text{ where } \Pi < \Omega \tag{A.3}$$

where f is the transform function, Ω is the dimension of our sample space,y is the vector of new features with reduced dimension Pi, and $\mathcal{R}$ is the sample or the feature space. The optimal linear features are calculated for two objective functions in this paper.

The first objective criterion is to preserve as much randomness (or variance) in

high dimensional space as possible using the Principal Component Analysis (PCA) or Karhunen-Loeve Transform (KL). The projection functions in PCA are defined by the first eigenvectors of the sample covariance matrix Σ_x [62].

Although there is no guarantee that the direction of maximum randomness contains good discrimination features, this method generally leads to good *signal* representations.

The second objective criterion is to preserve as much of class discriminatory information as possible using Fisher Linear Discriminant Analysis (LDA). The projected samples result more compact clusters. Let us consider that the projection results in J classes, where each of them contains N_j samples, then the center of the class C_j and the center of the complete set, C are:

$$\mu_j = \frac{1}{N_j} \sum_{x_i \in C_j} x_i \tag{A.4}$$

$$\mu = \frac{1}{N} \sum_{x_i \in C} x_i = \frac{1}{N} \sum_{j=1}^{J} N_j \mu_j \tag{A.5}$$

then, S_b is the *between classes scatter matrix*:

$$S_b = \sum_{j=1}^{J} N_j (\mu_j - \mu)(\mu_j - \mu)^T \tag{A.6}$$

and S_w is the *within classes scatter matrix*:

$$S_w = \sum_{j=1}^{J} \sum_{x_i \in C_j} (x_i - \mu_j)(x_i - \mu_j)^T \tag{A.7}$$

Then Fisher LDA projections are calculated by the first eigenvectors of the matrix $S_w^{-1} S_b$, maximizing the variance of the clusters while minimizing the variance of the projected sample points within each clusters [39]. As can be seen, if the discriminatory information is in the mean of the data, LDA generally results in better class

separability.

These two feature extraction methods are not the only methods. We shall see whether they are accurate enough for our estimation problem. The results of these classification techniques are addressed in the next section.

Simulation results and discussions

Table II shows the classification rates achieved by the above-mentioned classifiers, when we do not consider time dependency of the observation parameters.

Table III indicates the result of the same classifiers, when the time labels are incorporated in the observation vector. There are other nonlinear classifiers which may result in better classification rates. Nevertheless, the achieved classification rate of 92% practically suffices noise level predictions. PCA indicates which of the observation parameters have the most prominent impact on the predictability of the variation of noise power. It is observed that noise power level has a strong time-series component, which has more impact on our signal than random noise (i.e., distributional part). Statistical cross-validations among different test sets were performed to inspect and verify the absence of over-fitting in our predictors. Optimal receiver design incorporating the time series analysis is still an open problem (Even for the processes that are known and are fully controlled there is still ongoing debate about an optimal design).

The weather conditions may impact the telecommunication channel in two ways. If the precipitation causes the transmission line conductors to be wet, this may results in a drastic increase in corona noise generation. The climate condition also impacts the propagation constant. This analysis did not support further studying the strength of the association of these weather phenomena to the channel properties. The runtime snapshot comparison of the humid and rainy days to the sunny days indicate no

Table II. Results with time independent observations.

Classifier	Reduced Dimension	Classification Rate
Quadratic	No	0.29
KNN	No	0.38
Quadratic	PCA	0.25
Quadratic	LDA	0.29
KNN	PCA	0.75
KNN	LDA	0.33

major noise floor fluctuation with respect to the weather types and conditions, which anecdotally suggest that the noise floor variation is due to the Earth rotation, galactic sources or planetary atmosphere layers.

Figure 20 shows the variation of the transformer load (in Volt-Amperes) versus the noise level (in Volts) and scatter plot of 138KV transformer loading versus the noise level at 2.4 GHz frequency band (taken from a typical data set which is in conformity with other data sets). The plots in Fig. 4 may prematurely suggest the presence of causality between these two parameters. Through confirmatory study of the data sets, it is observed that there is basically no causality between the load pattern and the noise level but they just share a *common cause*, i.e., "time". Even though the load patterns of the transformers significantly differ in the residential subdivisions from the industrial regions, the recorded noise levels indicate identical patterns. Second, no significant changes in the classification rate were observed when we omitted the load pattern from the observation vector and deployed the best classifiers (This is due to the fact that the PCA de-correlates the data). In retrospective study, by

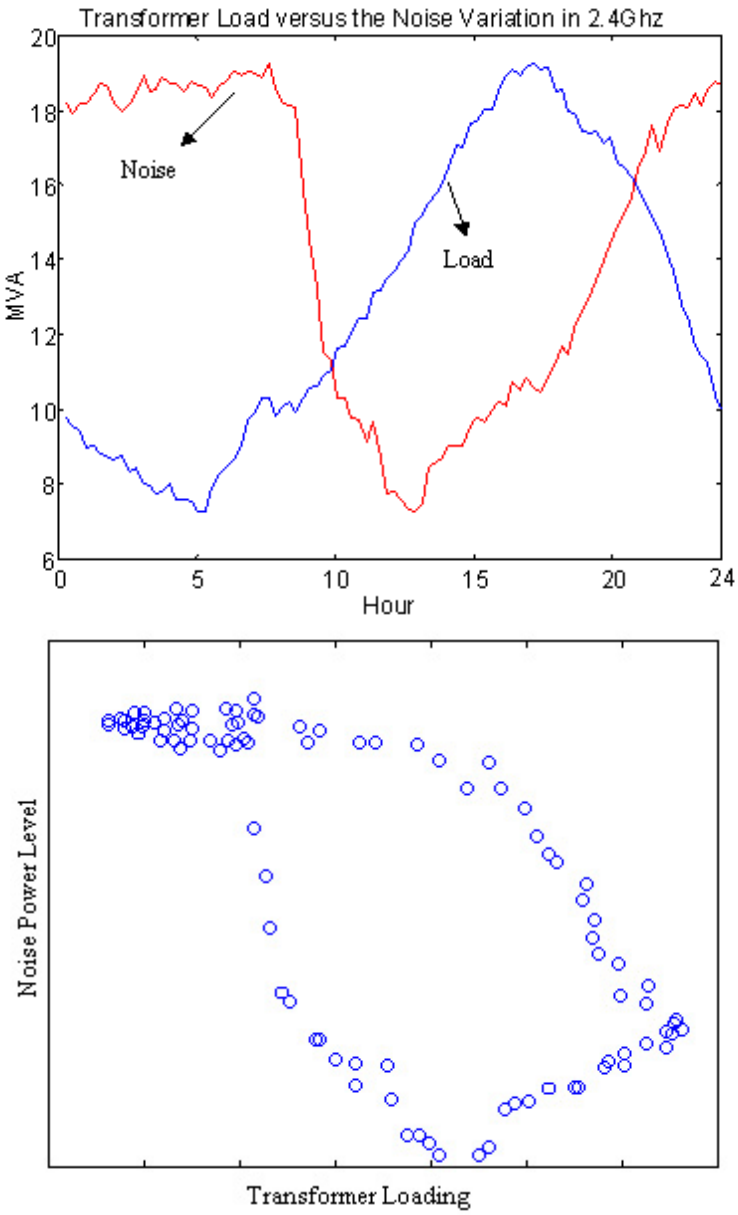

Fig. 20. The *variation* of the transformer load (in Volt-Amperes) versus the noise level (in Volts) and scatter plot of 138KV transformer loading versus the noise level at 2.4 GHz frequency band (taken from a typical data set which is in conformity with other data sets). The *absolute values* of the noise voltage level and the transformer loadings are not of concern in this analysis so the units have been taken off from this axis.

Table III. Results with time dependent observations.

Classifier	Reduced Dimension	Classification Rate
Quadratic	No	0.25
KNN	No	0.54
Quadratic	PCA	0.75
Quadratic	LDA	0.38
KNN	PCA	0.92
KNN	LDA	0.38

juxtaposing the experiment results in different substations, it appears that the noise power floor is associated with the substation voltage levels (which is almost constant during normal operations) but is not affected by the load pattern of the transformers. The slow change in the load pattern and the impact of the voltage levels on the noise floor are consistent with the theoretical equation of the conductor corona noise [53]. The comparisons of different test sets confirm similar findings in different substations.

In [2], it is shown that the noise variations over the time in a typical power-line substation are substantially different during the weekdays and weekends at 900MHz ISM frequency band (in particular in residential subdivisions). This observation may attribute to the interferences from other devices, e.g., cordless phones, government exclusive radios, etc., which operate at similar frequency band.

One can show with a simple calculation and using the simplified Friis equation that the path loss in 2.4 GHz is almost 8.5 dB higher than that of 900 MHz. This corresponds to less transmission range (and less interference range) at 2.4 GHz. By observing the collected data sets in this survey, it is confirmed that the data in

the substations that were located in the residential subdivisions indicated no major behavioral differences from the industrial, isolated or sparsely populated subdivisions at 2.4GHz. This observation is coherent to the theoretical path loss result regarding the inertness of interferences of distant devices in 2.4 GHz (even in the residential regions).

Worth mentioning is that according to the regulations [57], the primary users of 2.4 GHz spectrum are government systems and ISM users and the secondary (license-free) users are subject to strict output power in ISM frequency bands. Given the limited transmission range at 2.4 GHz and the consistency of the test results from several substation yards in different locations, it is suspected that the channel variations were due to the usage pattern of the *primary* users of this band. Nonetheless the interferences of the primary sources should be studied, which again demands for time-series analysis.

Moreover the deterministic variations of the noise floor have potential implications when no channel estimation and signal-level adjustments are performed. For instance in spread spectrum scenarios, the optimal performance of Direct Sequence Spread Spectrum (DSSS) systems often depends on the power control schemes in contrast with the Frequency Hopping Spread Spectrum (FHSS) schemes. By the same token in non-spread spectrum systems, amplitude dependant modulations such as QAM and ASK require more sophistication than the constant envelope career modulations such as CPFSK unless an adaptive power control scheme is applied, which incorporates the noise floor variation.

Conclusion

The noise sources and their behavior in extreme electromagnetic environment such as a power substation have been investigated in this survey. An experiment has

been designed to investigate the noise power variation and to cross-validate the probable confounding factors. Statistical analyses and confirmatory studies were done in attempts to ascertain the underlying associations. The underlying random and also semi-deterministic structure of the measured data suggests the inertness of the weather variations, ambient temperatures and load patterns. Using classification analyses, it is observed that the noise power had a strong time-series component, which had more impact on the channel than random noise (i.e., distributional part). Furthermore, it verifies the non-randomness of the noise floor and the possibility of noise floor estimation to some degree of certainty.

This suggests that the variation of the Signal to Noise Ratio (SNR) has a deterministic component, which optimally require more complex and adaptive schemes for certain types of modulations (e.g., QAM, ASK). The test methodology, measuring metrics selection and protection provisions adopted in this effort have applications in wireless design under high energy fields. It is also suggested that the field survey recommendation practices (e.g., [56]) be modified to include time series analysis.

Leaving aside the lack of extensive measurements and characterizations of wireless communication systems in high voltage substations in the literature, the experiments in this survey collectively support the applicability and the feasibility of wireless implementation in this environment.

APPENDIX B

EXTENSIONS TO TWO DIMENSIONAL ARRAYS

The discussion in Section B can be generalized to planar arrays and three dimension scenarios. Suppose that the sensors are placed at equispaced intervals on vertical and horizontal axes, Y and X, and θ and ϕ represent the spherical elevation and azimuth angles of arrival (Figure 21). Let us define $\zeta_x = d_x/\lambda$ and $\zeta_y = d_y/\lambda$, respectively, the

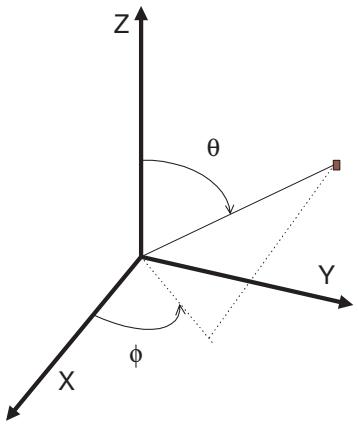

Fig. 21. The relation to the spherical coordinates.

horizontal and vertical element spacings per wavelength. If we define α and β such that:

$$\begin{aligned} \sin(\alpha) &= \sin(\theta)\sin(\phi) \ , \\ \sin(\beta) &= \sin(\theta)\cos(\phi) \ , \end{aligned} \tag{B.1}$$

and the true spherical elevation and azimuth angles are at θ_0 and ϕ_0 or equivalently

by the new conversion at α_0 and β_0, then the loci of the grating lobes will occur at:

$$\begin{aligned} \alpha_g &= \sin^{-1}\left(\sin\alpha_0 - \frac{\kappa_x}{\zeta_x}\right) , \\ \beta_g &= \sin^{-1}\left(\sin\beta_0 - \frac{\kappa_y}{\zeta_y}\right) , \end{aligned} \tag{B.2}$$

where $\{\kappa_x, \kappa_y\} = 1, 2, 3, \ldots$ (where available).

To avoid constructing maxima after histogram combining similar to the one dimensional array case, we should have

$$\begin{aligned} \alpha_{g1}|_{\zeta_x=\zeta_{p_x}} &\neq \alpha_{g2}|_{\zeta_x=\zeta_{q_x}} , \\ \beta_{g1}|_{\zeta_y=\zeta_{p_y}} &\neq \beta_{g2}|_{\zeta_y=\zeta_{q_y}} , \end{aligned} \tag{B.3}$$

for all possible dissimilar values of spacing per wavelengths relative to the horizontal axis and the vertical axis. Hence, the following inequalities should be satisfied:

$$\begin{aligned} \frac{\kappa_{x1}}{\zeta_{p_x}} &\neq \frac{\kappa_{x2}}{\zeta_{q_x}} , \\ \frac{\kappa_{y1}}{\zeta_{p_y}} &\neq \frac{\kappa_{y2}}{\zeta_{q_y}} , \end{aligned} \tag{B.4}$$

for any integers κ_{x1} and κ_{x2} ($\kappa_{x1} \neq \kappa_{x2}$) and κ_{y1} and κ_{y2} ($\kappa_{y1} \neq \kappa_{y2}$), which are constrained by (B.2).

APPENDIX C

SUFFICIENT CONDITION ON THE MINIMUM FREQUENCY SEPARATION OF THE SUBBANDS

Let us first define and review the following parameters and matrices:

1. θ is the parameter indicating the direction of the source and is unknown.
2. $\alpha = \sin\theta$ is unknown $(-\pi/2 \leq \theta < \pi/2)$.
3. $q(\alpha) = e^{-j\pi\alpha}$.
4. The set of the frequency subbands Ω, $\{\omega_l \in \Omega \mid l \in [1, L]\}$, is assumed known ($L$ is the total number of frequency subbands).
5. $\delta = \Delta\omega/\omega_1$ is known, real, scalar and is the minimum subband frequency separation or increments where ω_1 represents the lowest subband (center) frequency.
6. $m \in [1, M]$ is the m^{th} sensor element and the total number of sensors, M, is a known constant.
7. $Q_{ml}(\theta) = \left[e^{(m-1)\omega_l[-j\frac{d}{c}\sin\theta]}\right],\ m \in [1, M], l \in [1, L]$ is the steering matrix.
8. $\mathbf{S}$ = diag $[s_1(t)\ , s_2(t)\ , \ldots\ , s_L(t)]$, in which $s_l(t)$ is the signal vector at each subband.

Without loss of generality, let us assume that ω_l corresponds to the standard frequency of array. Then we have:

$$\mathbf{Q} = \mathbf{A}\ \mathbf{B}\ , \tag{C.1}$$

where

$$\mathbf{A} = \text{diag}\,[1\ , q\ , \ldots\ , q^{(M-1)}]\ , \tag{C.2}$$

$$\mathbf{B} = [q^{(l-1)(m-1)\delta}]\ \ m \in [1, M]\ ,\ l \in [1, L]\ . \tag{C.3}$$

Under noise free scenario, the output of the element would be:

$$\mathbf{U} = \mathbf{Q}\ \mathbf{S} = \mathbf{A}\ \mathbf{B}\ \mathbf{S}\ . \tag{C.4}$$

We want to know the condition on δ, if any, in order for the above equation to have consistent answers so that we can solve for α (note that as defined α is a bijective function of θ).

To answer the above question we need to start with the following proposition.

Proposition B.1. *Let D be the $M \times L$ matrix $[x^{(i-1)(j-1)}]$, where $x \neq 0$, and $M < L$. Then $rank(D) < M$ if and only if x is a k^{th} root of 1 for some $k \in \{1, 2, \ldots, M-1\}$.*

Proof. We show any grouping of M column vectors results in a matrix whose determinant is 0 if and only if x is a k^{th} root of 1 for some $k \in \{1, 2, \ldots, M-1\}$. We prove by induction on the number of rows, M, the case of $M = 1$ being trivial.

By using elementary matrices we may reduce the problem to that of considering the $(M-1) \times (L-1)$ matrix $[x^{i(j-1)}(x^i - 1)]$ and looking at all $(M-1)$ groupings of column vectors; in this case we consider the (1,1) minor of the matrix obtained by subtracting from each j^{th} column, $j > 1$, the $(j-1)$st column of D, and further by subtracting from each i^{th} row, $i > 1$, the first row of the resulting matrix.

Choosing the columns $j_1, \ldots, j_{M-1}$, where $j_\alpha \in \{1, \ldots, L-1\}$ and $j_\alpha \neq j_\beta$ for

$\alpha \neq \beta$, we consider

$$\begin{aligned}\left|[x^{i(j_\alpha-1)}(x^i-1)]\right| &= \left|([x^{i(j_\alpha-1)}])\right| \prod_{i=1}^{M-1}(x^i-1) \\ &= \left|([x^{(i-1)(j_\alpha-1)}])\right| \prod_{i=1}^{M-1} x^i \prod_{i=1}^{M-1}(x^i-1), \end{aligned} \tag{C.5}$$

where $|\ .\ |$ denotes the determinant operation. Using the induction hypothesis on the first term in (C.5), we see the right hand side of (C.5) is 0 if and only if $x^i = 1$ for some $i \in \{1, \ldots, M-1\}$. This completes the proof. □

Corollary B.2. *$rank(U) < M$ if and only if $\alpha = \frac{2n}{k\delta}$ for some $k \in \{1, \ldots, M-1\}$ and $n \in \{-\left\lfloor \frac{k}{2} \right\rfloor, \ldots, \left\lfloor \frac{k}{2} \right\rfloor\}$.*

Proof. $rank(U) = rank(Q) = rank([(q^\delta)^{(i-1)(j-1)}]$. Then apply Proposition (B.1) with $x = q^\delta$. □

Corollary B.3. *$rank(U) = M$ if and only if $\delta < \frac{2}{M-1}$.*

Proof. Direct result from Corollary (B.2). □

Hence the matrix B and consequently U would be full rank if and only if $\delta = \frac{\Delta\omega}{\omega_1} < \frac{2}{M-1}$.

APPENDIX D

THE PROBABILITIES OF THE GRATING LOBES AND THE TRUE ANGLE REQUIRED FOR THE MSE APPROXIMATE

Let us start by using the decision statistics that was derived in Equation (3.11), we start the derivations based on the decision statistics

$$J(\theta_l) = Tr(Q_l(\theta)\ Q_l^T(\theta)\ \hat{R}_l)\ , \tag{D.1}$$

to find the true angle in terms of

$$\hat{\theta}_l = arg\left\{\max_\theta\ Tr\ (Q_l(\theta)\ Q_l^T(\theta)\ \hat{R}_l)\right\}\ . \tag{D.2}$$

Given the assumption on the discretized grating lobes addressed in Chapter V, the probability that the true angle θ_0 is chosen rather than other κ_{θ_0} grating lobes, θ_κ, would be:

$$\Pr(\theta_l = \theta_0) = 1 - \Pr\left\{\bigcup_{\kappa=1}^{\kappa_{\theta_0}}\Big(J(\theta_\kappa) > J(\theta_0)\Big)\right\}\ . \tag{D.3}$$

One can use the *Bonferroni inequalities* to find lower and upper bounds for the union term in the right hand side of the above equation. To do so, let us define:

$$P_1 = \sum_{\kappa=1}^{\kappa_{\theta_0}} \Pr\Big(J(\theta_\kappa) > J(\theta_0)\Big)\ , \tag{D.4}$$

$$P_2 = \sum_{\kappa_1<\kappa_2}^{\kappa_{\theta_0}} \Pr\ \Big\{\ \Big(J(\theta_{\kappa_1}) > J(\theta_0)\Big) \cap\ \Big(J(\theta_{\kappa_2}) > J(\theta_0)\Big)\ \Big\}\ , \tag{D.5}$$

and for $2 < j < \kappa_{\theta_0}$,

$$P_j = \sum \Pr\ \Big\{\ \Big(J(\theta_{\kappa_1}) > J(\theta_0)\Big) \cap \cdots \cap\ \Big(J(\theta_{\kappa_j}) > J(\theta_0)\Big)\ \Big\}\ , \tag{D.6}$$

where the summation is taken over all j-tuples of distinct integers. Then, for odd

$j \geq 1$, the upper bound would be,

$$\Pr\Big\{ \bigcup_{\kappa=1}^{\kappa_{\theta_0}} \Big(J(\theta_\kappa) > J(\theta_0) \Big) \Big\} \leq \sum_{i=1}^{\kappa} (-1)^{i+1} P_i \ , \tag{D.7}$$

and for even $j \geq 2$, one can find the lower bound as,

$$\Pr\Big\{ \bigcup_{\kappa=1}^{\kappa_{\theta_0}} \Big(J(\theta_\kappa) > J(\theta_0) \Big) \Big\} \geq \sum_{i=1}^{\kappa} (-1)^{i+1} P_i \ . \tag{D.8}$$

If we implement the first order approximation by setting $j = 1$, we eliminate the intersection terms and we achieve the famous *Boole's inequality* or the *Union Bound*. This implies ignoring the events in which the probability of simultaneous occurrence of two or more grating lobes are higher than that of the true angle. Given the equiprobable assumption of the grating lobes[1], we can easily derive a more precise expression of the union term in Equation (D.3). We can calculate the probability of simultaneous occurrence of j-tuples, using the *binomial distribution*:

$$\Pr(\text{any j-tuple}) \propto \mathcal{B}(\kappa_\theta, \frac{j}{\kappa_\theta}). \tag{D.9}$$

So we can express the union term in the right–hand side of Equation (D.3) and the probability of the true angle with a desirable accuracy.

The remaining term to be calculated is the pairwise probability:

$$\Pr(\theta = \theta_\kappa) = \Pr\Big\{ \Big(J(\theta_\kappa) > J(\theta_0) \Big) \Big\} \ , \tag{D.10}$$

which is the probability of choosing a grating lobe. Equation (D.10) can be written

[1]We can still achieve a more precise expression by incorporating a priori information in Equation (2.17).

as:

$$\Pr(\theta = \theta_\kappa) = \Pr\left\{\left(J(\theta_\kappa) > J(\theta_0)\right)\right\} \tag{D.11}$$

$$= \Pr\left\{\left(J(\theta_\kappa)^2 > J(\theta_0)^2\right)\right\} \tag{D.12}$$

$$= \Pr\left\{\left(J(\theta_\kappa)^2 - J(\theta_0)^2\right) < 0\right\} \tag{D.13}$$

$$= \Pr\left\{Tr\Big(\{Q_l(\theta_k)\ Q_l^T(\theta_k) - Q_l(\theta_0)\ Q_l^T(\theta_0)\}\ \hat{R}_l\Big) < 0\right\} \tag{D.14}$$

$$= \Pr(D < 0) \tag{D.15}$$

where we considered D as the new decision variable,

$$D = J(\theta_\kappa)^2 - J(\theta_0)^2\ . \tag{D.16}$$

We can use the criterion (3.33) discussed in Section E of Chapter III to further simplify (D.14). Equation (D.1) together with (D.16) construct a *quadratic form*, analogous to the known problem of M–ary non-coherent detection of binary signaling under AWGN. The grating lobes and the true angles can be interpreted as the matched output to any M–ary signal waveform. The general quadratic form of this equation has been discussed in [64, Appendix B], in which the general quadratic expression takes the form:

$$D = \sum_{n=1}^{N}(A|J_{\theta_\kappa}(n)|^2 + B|J_{\theta_0}(n)|^2 + CJ_{\theta_\kappa}(n)J^*_{\theta_0}(n) + C^*J_{\theta_\kappa}(n)^*J_{\theta_0}(n))\ , \tag{D.17}$$

where the constants for the problem at hand becomes $A = 1$, $B = -1$ and $C = 0$, and $J^*_{\theta_0}(n)$ and $J_{\theta_\kappa}(n)$ are respectively the outputs of the receiver corresponding to the true direction and the grating lobe at sample n, with the following moments (consult

with Section II for the mathematical model):

$$\begin{aligned} E(J_{\theta_0}) =& Ms(n) \ , \\ E(J_{\theta_\kappa}) =& Q_{\theta_\kappa}^H Q_{\theta_0} s(n) \ , \\ Var(J_{\theta_0}) =& M\sigma_n^2 \ , \\ Var(J_{\theta_\kappa}) =& M\sigma_n^2 \ , \\ Cov(J_{\theta_\kappa}, J_{\theta_0}) =& Q_{\theta_\kappa}^H Q_{\theta_0} \sigma_n^2 \ . \end{aligned} \tag{D.18}$$

Furthermore let us define:

$$\begin{aligned} S \equiv& M \sum_{n=1}^{N} |s(n)|^2 \ , \\ R_0 \equiv& |Q_{\theta_\kappa}^H Q_{\theta_0}| \ . \end{aligned} \tag{D.19}$$

Following similar straightforward algebra in [64, Appendix B] and plugging in the parameters, we arrive at the following result for $N = 1$ snapshot:

$$\Pr(\theta = \theta_\kappa) = Q(\nu_1, \nu_2) - \frac{\nu_3}{\nu_3 + \nu_4} I_o(\nu_5) \ e^{-\frac{1}{2}(\nu_1^2 + \nu_2^2)} \ , \tag{D.20}$$

where I_o is the zeroth order *modified Bessel function* and Q is the *Marcum Q-function* defined as:

$$Q(a, b) = \int_b^\infty xe - \frac{x^2 + a^2}{2} \mathcal{I}_o(ax) dx \ , \tag{D.21}$$

and where:

$$\nu_1 = \sqrt{\frac{S}{2\sigma_n^2}(1 - \sqrt{1 - MR_0^2})} \ , \tag{D.22}$$

$$\nu_2 = \sqrt{\frac{S}{2\sigma_n^2}(1 + \sqrt{1 - MR_0^2})} \ , \tag{D.23}$$

$$\nu_3 = \sqrt{1 + MR_0^2} \ , \tag{D.24}$$

$$\nu_4 = \sqrt{1 - MR_0^2} \ , \tag{D.25}$$

$$\nu_5 = \frac{SR_0}{2\sigma_n^2} \ . \tag{D.26}$$

The interested reader may consult with [64] and incorporate Equations (D.18) and (D.19) for the problem of $N > 1$ snapshots.

The pairwise probabilities for all grating lobes need to be calculated and substituted in Equation (D.3) to achieve the probability that the true angle is θ_0.

VITA

Alireza Shapoury received his B.S. and M.S. degrees from Shahid Beheshti University and Iran University of Science and Technology both in electrical engineering, in 1994 and 1997, respectively. Since 2000 he has been working toward his Ph.D. degree in Electrical Engineering at Texas A&M University, in College Station, Texas. He received his Ph.D. in August 2007. His research interests include channel estimation, RF/mixed signal measurement techniques and antenna array processing. Alireza can be reached at 1124 East Potomac Lane, Palatine, IL 60074, or via email at shapoury@ieee.org.

This dissertation was typed in LaTeX by Alireza Shapoury